Analysis and Forecast of Two Storms Characterized by Extreme Deepening Rates

Submission to Mon. Wea. Rev. 2003.02.14

Oreste Reale [1]

Lars Peter Riishojgaard

Goddard Earth Sciences and Technology Center,
University of Maryland Baltimore County,
and
Data Assimilation Office, NASA Goddard Space Flight Center, Greenbelt,
Maryland

[1]Corresponding author's address: NASA Goddard Space Flight Center, Code 910.3, Greenbelt, MD 20771, Email oreale@dao.gsfc.nasa.gov

Abstract

Between 25 and 27 December 1999 two very intense cyclones, named Lothar and Martin, swept across northern and western France causing substantial life and property loss. In this work, the finite volume general circulation model and data assimilation system (fvDAS) developed at the Data Assimilation Office of the NASA Goddard Space and Flight Center is being used to investigate these storms.

In the first part of this article the dynamics of the storms is analyzed, and some important mechanisms are unveiled.

The second part describes a set of eleven data assimilation experiments to study the impact of different data types on the automated analyses. Cloud-track winds provided by EUMETSAT and surface winds from QuikSCAT are being used. These data are assimilated with a range of different parameter settings of the forecast error covariance model.

The results show that generally the additional wind data set have positive impacts on the analyses: particularly, the analysis of Lothar can be slightly improved by using the Eumetsat winds, and the analysis of Martin can be strongly improved by using the full-resolution QuikSCAT winds with a more localized influence.

The third part of this article is focused on the forecast of Lothar which is very well predicted in the 1-5 day range by the fvDAS system.

The deterioration of the forecast experienced by other operational numerical weather models at the short range (1-3 days) seems less pronounceed in the fvDAS. However, further improvement at the very short range (1 day) is obtained by assimilating the Eumetsat high resolution winds and also, to a lesser extent, the QuikSCAT winds. No positive impact is detected when these data sets are used for a longer range forecast.

Finally, these results are interpreted in the frame of the dynamics of the two storms. It is found that the dynamics of Lothar is predominantly driven by the jet stream and it is extremely baroclinic, whereas Martin appears to be the result of an unusual synergy between an anomalous low-level jet and the jet stream. These different mechanisms are possibly responsible of the particular response of the fvDAS system in the two cases.

1 Introduction

On 26 December 1999 and during the evening of 27 December 1999, two extraordinary storms affected western and central Europe. The two storms were named Lothar and Martin, respectively, by the German Weather Service (Deutsche Wetterdienst, DWD), and they have sometimes been referred to as to the '1999 French storms' although their devastating effects were not confined to France. Both storms were characterized by exceptionally high deepening rates (part of which was observed over land), propagation speeds on the order of 100 $km\,h^{-1}$, lack of substantial convection, little or moderate observed precipitation and very strong winds (up to 55 $m\,s^{-1}$). Operational numerical models used by weather forecasting centers performed poorly.

Although Lothar and Martin are in many respects exceptional, fast-developing, devastating winter cyclones are not uncommon over western and northern Europe. In general, the occurrence of such storms pose several problems to the numerical weather prediction community. The most immediate problem is the intrinsic limitation in predictability due to uncertainties in the initial conditions. The initial conditions are difficult to establish because of the rapidly developing dynamics generally associated with extreme deepening rates. This is illustrated e.g. in the work of Hello et al. 2000, focused on a somewhat similar event: a system referred to as the 'Christmas storm' that affected the British Isles one year earlier, between 24 and 25 December 1998.

An additional and related problem is that of establishing a validating analysis. In fact, for any performance evaluation of a model forecast it is desirable to have an objective validating analysis of the event one wants to simulate: this analysis is considered the 'truth' against which various forecast experiments can be scored. However, if the analysis does not reproduce the event sufficiently well, any attempt to objectively rate the quality of the forecast will be flawed. The study of Lothar and Martin provides good examples of this problem since it has been generally accepted that the objective analyses of the fully developed storms are unsatisfactory (Ulbrich et al. 2001). As a consequence, one study that makes experiment forecasts does not adopt any objective analysis as 'truth', but rather chooses as 'truth' a 48-hour forecast, subjectively considered good after comparison with sea level pressure maps (Leutbecher et al. 2002).

The first goal of this article is to establish the best possible analysis of Lothar and Martin, given the characteristics and limitations of the assimilation system used. In order to design a proper strategy to produce better analyses of these storms, we first investigate the their dynamics and isolate what we believe to be important cyclogenetic mechanisms. The importance of an upper-level jet, already found by previous authors (Wernli et al. 2002) is confirmed. Moreover, we find an interesting feature that does not appear to have been observed before: a low-level jet, centered at about 900-850 hPa, associated with the storm Martin. This low-level jet follows, and is perfectly

parallel to, the upper-level jet stream, affecting the transversal circulation related with the entrance region of the upper-level jet streak, during the entire phase of development of Martin.

To see if more information on these two jets could have a positive impact, two data sets are considered: the high resolution atmospheric motion vectors (provided by Eumetsat, hereafter referred to as EW), which are upper-level cloud-track based geostationary winds, and the NASA QuikSCAT winds (hereafter QW), which are near-surface level marine winds.

Then, we see how the assimilation process can impact the storm representation in the automated analyses. This is being done with a set of eleven assimilation experiments, run with the NASA Data Assimilation Office finite-volume Data Assimilation System (fvDAS). In these experiments, we turn on or off the assimilation of EW and the 'thinning' of QW, we perturb the influence of observations by modifying their correlation function support (using the error covariance model developed by Gaspari and Cohn 1999) and by changing the weight given to the observations in the analysis, through changing the forecast error variance.

In spite of the extreme intensity and proximity in time of Martin and Lothar, we find that the respective dynamic mechanisms for their development appear to be totally different, and consequently, also the behavior of the assimilation system is very different in the two cases. Lothar appears to be quite well predicted in the 24-120 hour range, even though the automated

analysis of Lothar is very unsatisfactory, both when compared to the actual observations and when compared to earlier forecasts. Martin, on the other hand, is represented quite well in the analysis, but it is totally missed in the forecast at all ranges.

The results of the assimilation experiments show that Eumetsat and full-resolution QuikSCAT Data generally have a positive impact on the automated analysis of both storms. However, in the case of Lothar, the best results are produced by assimilating the EW winds with a narrower background error correlation (thus making the impact more local), but, at the same time, giving more weight to the observations. The best result for Martin is obtained by using the QuikSCAT data at their full resolution and with narrower background error correlation. The reason is that lower-level processes seem to be more important in the case of Martin and hence that observations pertaining to the lowest levels of the model are of most benefit.

Finally, a series of forecasts of Lothar are performed. The control run is quite satisfactory. Unlike the European Center for Medium Range Forecast (ECMWF) model, which was able to predict the storm at a 120 hour range but had a poor representation on the short time scales (Leutbecher et al 2002), the fvDAS maintains a very good performance even at 24 hours. However, an interesting result is that satellite data (QuikSCAT and geostationary winds) can further improve the forecast, but only in the short range. In particular, the 24 hour forecast for Lothar is substantially improved by

including the Eumetsat winds. The QuikSCAT winds also have a positive impact on the short range forecast, when used in conjunction with narrower forecast error correlations. Full resolution QW or EW used for forecast in the 3-day or longer range have generally a negative impact.

2 Synoptic Discussion

2.1 The large scale forcing

A remarkable planetary-scale jet stream activity during the days preceding the development of the storms characterizes the entire northern hemisphere. Figure 1 shows the wind speed at 300 and 900 hPa as well as the sea level pressure (slp) between 21 and 24 December 1999. The analyses are produced by the fvDAS in the standard configuration (control run, named EXP1). The subsequent figures, unless otherwise specified, are based on this run. An anomalous jet stream with a jet-streak maximum of more than 100 ms^{-1} can be seen over the northern Pacific at 1200 UTC 21 December. Following the jet stream path downstream from eastern Asia towards the East, it can be seen that a 900 hPa jet, stretching from 25^oN to the Gulf of Alaska with maximum speeds exceeding 40 $m\,s^{-1}$ connects the jet over the Pacific with the entrance region of a strongly anticyclonically-curved upper-level jet that dominates most of the northwestern part of North America. A cyclone occurs over the Hudson Bay and an upper-level jet stream is originating over the Great Lakes. At 1200 UTC 22 December, it should be noted that:

- The low-level jet connecting the jet stream over the Pacific with the anticyclonically curved jet over north-western North America has weakened significantly
- The maximum speed over the anticyclonically-curved jet has moved rapidly clockwise along the jet stream
- The cyclone over the Hudson Bay has deepened
- The jet exiting from the US East coast has significantly strengthened

At 1200 UTC 23 December, the jet over northwestern North America weakens, whereas the jet exiting from the East coast of North America strengthens and rapidly propagates across the Atlantic.

By 1200 UTC 24 December, the low-level jet over the Pacific, and upper-level jet over the American continent have almost disappeared, whereas the jet stream over the Atlantic has gained comparable strength (speed maximum of about 100 $m\,s^{-1}$) with the jet stream over the Pacific.

This sequence of events suggests that a transfer of energy from the Pacific to the Atlantic jet stream may have occurred on the 21st and the 22nd. Vertical cross-sections of temperature, vorticity and wind (not shown) support the possibility of some dynamic coupling between the tropopause level and the 900 hPa jet over the Pacific at 1200 UTC 21 December, between the 900 hPa jet over the Pacific and the upper-level anticyclonically curved jet over northwestern North America and finally between the anticycloni-

cally curved upper-level jet and the Atlantic jet, via the low level thermal advection induced by the cyclone over the Hudson Bay.

2.2 The Atlantic jet stream

Once the Atlantic jet stream is well established, its most striking characteristics, apart from the uncommon speed of up to more than 100 $m\,s^{-1}$, are its very large scale and the apparent presence of some mechanism that inhibits the release of instability, during the 36 hours preceding the explosive cyclone development. Once this mechanism, which will be the subject of a later discussion, ceases to be effective, there is a dramatic transfer of kinetic energy from the jet level to the surface cyclone, leading to a surface deepening rate on the order of 30 hPa over *six* hours. In Figure 2, the 300 hPa wind is shown together with the sea level pressure and the 900 hPa wind over the North Atlantic. At 0000 UTC 25 December 1999 (Figure 2a), the very strong upper level jet stream stretches from the southestern part of the US to western Europe. The anomalous feature of it is that it seems to follow a straight path, with no tendency to create meanders or short waves of any kind. This is particularly remarkable considering that the jet extends over more than 90^o in longitude and is therefore to be regarded as a planetary-scale structure. At about 50^oW, at the right entrance region of the jet, a moderate cyclone can be seen. This is the early stage of what would eventually become the storm Lothar. Indeed, a circulation can be inferred from ship observations already at 1200 UTC 24 December at approximately 60^oW (not shown). Be-

tween 1200 UTC 25 December and 0000 UTC 26 December, Lothar crosses the Atlantic: it can be seen at 30^oW and 10^oW respectively (Figures 2b,c), continuing to propagate at a speed on the order of 100 $km\,h^{-1}$. At the same times a broad but weak cyclone can be seen at about 60^oW and 50^oW respectively. This is the onset of Martin. At 1200 UTC 25 December and 0000 UTC 26 December, it is important to note the low-level jet to the south of the upper-level jet, almost parallel to it. This low-level wind maximum will play a significant role in the subsequent development, as it will be shown later. At 1200 UTC 26 December (Figure 3a) Lothar has almost made landfall, Martin has accelerated to the same speed of Lothar, being located at about 40^oW, the upper jet level has reduced its intensity, and the 900 hPa jet has strengthened to 30 $m\,s^{-1}$ in proximity of Martin, still retaining a parallel orientation with respect to the upper level wind. At 0000 27 December (Figure 3b) Martin has propagated about 10^o eastward, the wind speed at the upper level jet level has further decreased and the low-level jet has increased to a maximum speed of more than 40 $m\,s^{-1}$. At 1200 UTC 27 December (Figure 3c) Martin is close to landfall, the upper level jet has further reduced its intensity (it almost disappears over the subsequent few hours, not shown) and the 900 hPa jet to the south of Martin now peaks at almost 50 $m\,s^{-1}$.

These figures suggest some form of cooperative interaction between the upper level and the low-level jet, or transfer of kinetic energy from the upper to the lower jet. This idea will be discussed later.

2.3 Lothar and Martin in the sea level pressure and 500 hPa analyses

In Figure 4, the sea level pressure (slp) and 500 hPa geopotential height fields are shown, as they appear in the fvDAS analyses. The most remarkable aspect is the apparent lack of wave activity in the 500 hPa field. Indeed, between 1200 UTC 25 December and 0600 UTC 26 December, the surface pressure center appears to travel eastward at the speed of about 100 $km\,h^{-1}$ ahead of a large scale slightly *anticicylonically curved* 500 hPa flow, therefore in an area of negative vorticity advection. The lack of a trough at 500 hPa on the ECMWF analyses was noted also by Wernli et al. (2002) leading the authors to conclude that the storm was 'shallow'. The second remarkable aspect is that the slp map displays a closed circulation at 0600 UTC 25 December 1999, but only a trough six hours later, and an even less-pronounced trough at 1800 UTC 25 December and 0000 UTC 26 December. It is possible though that both these features in the analyses (the apparent 'shallowness' due to lack of any wave in the mid-troposphere, and the apparent weakening between 1200 UTC 25 December and 00 UTC 26 December) are caused by a lack of data or rejection of critical data.

In Figure 5a,b one can see the rapid propagation of Lothar across France and Germany between 0600 and 1200 UTC 26 December 1999, although the analyses do not show a closed circulation but portray Lothar only as a short wave. Land surface observations will be shown later for comparison. Fig-

ures 5c,d display at these times a well-defined 500 hPa short wave associated with the motion of Lothar. We speculate that the change from 1800 UTC 25 December (Figure 4f) in which no short wave is seen, is due not to dynamical reasons (as argued by Wernli et al. 2002) but to the fact that Lothar moved from an area with little or no data coverage at 500 hPa (at 1800 UTC 25 December), to an area over land with abundant upper-air observations. In Figure 5e Martin can be seen at about 25^oW, and there is again an apparent lack of any feature at 500 hPa (Figure 5f) at 1800 UTC 26 December 1999. Subsequently, the slp trough associated with Martin deepens significantly and, at 00 UTC 27 December, a hint of a trough can be seen also at 500 hPa (Figures 5g,h). In the following hours, however, a very well-defined cyclone, with a minimum of about 970 hPa, and a clear circulation appear in the fv-DAS analyses, together with a sharp 500 hPa trough, that rapidly develops as soon as the storm is over the continent (Figure 6).

In both storms a strong development of the mid-tropospheric features occurs as soon as the storm goes over land, where vertical wind profiles start becoming available to the data assimilation process. It is possible then that the supposed 'shallowness' of the storm over the ocean is caused not by the particular dynamics of this storm but simply by a lack of mid-tropospheric data which is particularly damaging because of the very high propagation speed of the system.

Even though the mid-troposphere might be misrepresented in both storms,

there is a marked difference in the surface representation of Lothar and Martin. It will be shown later that, in spite of the comparable size and depth of the observed surface low, the analyzed representation of Martin is much more satisfactory than the one of Lothar. In fact, the automated analysis display a very well-defined closed low in Martin case.

In Figure 7a the National Oceanic and Atmospheric Administration (NOAA) infrared satellite image at 04:37 UTC is shown, at a time in which the center of Lothar is located over northern France, close to the English Channel. The dense cirrus shield between southeastern England and Belgium is associated with the center of Lothar. However, it is interesting to note that only poorly organized cloudiness is present over some areas of central-northern France where at the same time very high wind speeds are being recorded.

Figure 7b shows the NOAA infrared satellite image at 19:01 UTC 27 December. The center of Martin is clearly coincident with the center of a low-level cloud vortex over northwestern France. To the north of a sharp border of upper clouds, indicating the jet stream, only low and mid-level clouds can be seen. The absence of any substantial convection or high level clouds at the vortex scale is remarkable.

The difference between the height of the clouds, as it appears in the two images, near the respective centers of the two storms (Figures 7a and 7b) is evident. Over Lothar, the cirrus shield and some convective cloudiness are indicative of a dynamics in which there might be some contribution from

latent heat release, as confirmed also by model diagnostics in Wernli et al. (2002). Conversely, the low-level cloud vortex which well delineates the cyclonic circulation of Martin, is suggestive of a relatively dry dynamics.

2.4 Comparison with surface observations

In Figure 8a, observed sea level pressure values are displayed, at about the time of maximum intensity for Lothar (at 0600 UTC 26 Dec). The subjectively estimated position of Lothar is marked with 'L'; its minimum was confirmed to be 961 hPa by the DWD (Wernli et al. 2002). The six-hour tendency of the observed sea level pressure, and the analyzed sea level pressure field at the same time, are shown in Figure 8b. The slp analysis is very unsatisfactory. No closed circulation can be seen, and only a broad trough appears in the analysis in correspondence to Lothar. Moreover, the sea level pressure difference between observed values and analysis is about 20 hPa. It is important to note that the area of largest analysis error corresponds to a six-hour decrease in slp of more than 30 hPa (up to 38 hPa close to the center). The analysis improves slightly at 1200 UTC (Figures 8c,d).

For Martin, the situation is different. The observed slp at 1800 UTC 27 December is shown in Figure 9a, and the corresponding estimated position of the storm (at that time of 962 hPA) is marked with 'M'. There is good agreement with the analysis in Figure 9b: there is a very well-defined minimum, although its center is misplaced by about 1^o to the north, and the minimum analyzed pressure is about 10 hPa higher than the lowest observed pressure.

The analysis at the following time, 0000 UTC 28 December, is indeed quite satisfactory (Figures 9c,d).

3 The Experiments

3.1 The Model

The experiments described in this paper were run using the so-called finite-volume data assimilation system (fvDAS) developed in the Data Assimilation Office at the Goddard Space Flight Center. The fvDAS is a sequential analysis system in which the atmospheric state is carried forward in time by a global numerical weather prediction model, and the Kalman filter analysis equation is solved at each synoptic time by the so-called Physical-space Statistical Analysis System (PSAS, Cohn et al., 1997). The dynamical core of the forecast model is based on Lin and Rood (1996) and the physics parameterizations are from the NCAR Community Climate Model (CCM3). The work described here was carried out using version 1.2r5 of the fvDAS, with the forecast model being run at a horizontal resolution of $1^o \times 1.25^o$ and 55 layers in the vertical, while the analysis increments are calculated at a resolution of $2^o \times 2.5^o$ and 25 levels.

3.2 Motivation and experiment design

The overall dynamical context given above suggests that an accurate representation of both the upper-level jet and the low-level jet over the Atlantic

in days prior to the development of the storms will be necessary in order for the system to analyze and forecast these two cyclones. A number of factors contribute to the difficulty of representing these features and the subsequent development correctly in a data assimilation system: the relative narrowness of the jet streams (and consequently the strong shears at the edges), the high propagation speeds both of the jet streaks and of the surface features (recall that the surface lows travel at a speed of about 30 $m\,s^{-1}$), and deepening rates of the order of 30 hPa over six hours and up to 10-20 hPa in the hour preceding the minimum for several land stations. One of the main purposes of the work presented here is to investigate the possible impact on the model simulation of the storms of different representations of the two jets. In order to test this, a number of experiments were carried out, some in which additional observational datasets were introduced (High-resolution geostationary satellite winds provided by EUMETSAT, and high-density surface winds obtained by QuikSCAT, respectively), others in which certain parameters of the forecast error covariance model were subject to variations.

Generally, the forecast (or background) error covariance controls the shape and magnitude of the impact of a given observation on the analysis. The scalar gain factor K controls the amount by which the analysis is drawing to an observation at its location and is given by

$$K_s = \frac{\sigma_f^2}{\sigma_f^2 + \sigma_o^2}, \tag{1}$$

where σ_f^2 and σ_o^2 is the error variance of the forecast and of the observations, respectively. The gain factor lies in the interval between 0 and 1, with $K = 0$ implying that the observations are being ignored due to their infinite uncertainty, and $K = 1$ corresponding to direct insertion of observations due to infinite uncertainty of the background forecast. For the mass variable, the standard version 1.2r5 of the fvDAS prescribes a constant scalar gain of $K = 0.6$. For the case discussed here, bracketing experiments with $K = 0.5$ and $K = 0.7$ were carried out.

The forecast error correlation controls the extent and the shape of the impact of an observation at points away from the observation location itself. In the fvDAS, the forecast error correlation is modeled as proposed by Gaspari and Cohn (1999). The correlation model has compact support, i.e. it goes exactly to zero beyond a certain distance, R, which in turn is coupled to the correlation length scale, L. In practice, this means that for a given point in the domain, all observations obtained at points that are within a distance of R will have an impact on the analysis at that point. The background error correlation thus acts as a spatially averaging filter on the analysis increment. For an observing system which is sparsely distributed horizontally, one could argue that is advantageous to use a relatively long length scale both in order to spread the observational information as much as possible and in order to avoid local shocks to the assimilation system. On the other hand this also means that particularly in a situation with strong gradients in say, the wind

field, a substantial part of the analysis impact at any given point may come from observations from relatively far away that are not necessarily representative of the local flow. In the standard configuration of the fvDAS, the distance of support is set to $R = 6000\ km$. In order to test the impact on the representation of the jet streams, experiments were carried out with a reduced support of $R = 3000\ km$.

In a multivariate analysis system such as PSAS, observations pertaining to the mass field will have an impact on the flow field and *vice versa*. The exact form of this impact is controlled by the wind/mass balance built into the background error covariance model. In fact, since the mass field is generally better observed than the flow field, much of the information added to the flow field in the analysis is derived from mass observations. In the work described here, we are focusing on the representation of the flow field in particular, so in order to test whether the representation of the two jet streams could be improved by using additional direct (or at least less indirect) wind observations, experiments were carried out using additional upper-air winds obtained by feature-tracking in geostationary satellite imagery provided by EUMETSAT. Furthermore, experiments were carried out in which QuikSCAT surface winds over the ocean provided by NASA were analyzed at a density that was substantially higher than in the standard fvDAS configuration. In the standard configuration, the pre-analysis data processing reduces the more than 20,000 QuikSCAT measurements of zonal and merid-

ional wind to about 2400, or approximately 12% of the original number. In the experiments in which the QuikSCAT data reduction is disabled, all the observations are retained.

In summary, the default condition, used in the control run (EXP1) is provided by K=.6, $R = 6000\ km$, no EW assimilation and 'thinned' QW. Experiments are performed in which K is changed from .6 to .7 or .5, R is reduced from 6000 km to 3000 km, EW assimilation is enabled or disabled, and QW thinning is enabled or disabled. Table 1 summarizes all the experiments that have been conducted. The ten-day control run is initialized at 0000 UTC 21 December 1999 and all the other simulations are performed starting from the same date.

To avoid overlapping of effects due to non-linearities, we analyze the output of these experiments, focusing on the differences that occur between simulations which differ only for one parameter at a time. Therefore, we compare couples of experiments among which only one parameter is changed, to investigate the following impacts (see Table 1)

1. Impacts of the Eumetsat winds

   - EXP2 versus EXP1: impact of assimilating EW at R=6000, K=.6
   - EXP3 versus EXP9: impact of assimilating EW at R=3000
   - EXP4 versus EXP8: impact of assimilating EW at K=.7

2. Impacts of the un-thinned QuikSCAT winds

- EXP11 versus EXP1: impact of higher density QW at R=6000, K=.6
- EXP13 versus EXP9: impact of higher density QW at R=3000

3. Impact of smaller support with Eumetsat winds
   - EXP3 versus EXP2: impact of reducing R, when K=.6 and EW are assimilated
   - EXP5 versus EXP4: impact of reducing R, when K=.7 and EW are assimilated
   - EXP7 versus EXP6: impact of reducing R, when K=.5 and EW are assimilated
4. Impact of smaller support without Eumetsat winds
   - EXP9 versus EXP1: impact of reducing R when K=.6 and EW are not assimilated
5. Impact of variable K with Eumetsat winds
   - EXP6 and EXP4 versus EXP2: impact of variable K at R=6000 and when EW are assimilated
6. Impact of variable K without Eumetsat winds
   - EXP8 versus EXP1: impact of variable K at R=6000 and when EW are not assimilated

7. Impact of smaller support with un-thinned QuikSCAT winds

   - EXP 13 versus EXP 11, impact of variable R at K=.6, when QW are at full density

4 Experiment results

4.1 General discussion

The impact of the experiments described in Table 1 is evaluated as the objective difference of slp and geopotential height at 900 hPa, at 0600 and at 1200 UTC 26 December for Lothar, and at 1800 UTC 27 December and 0000 UTC 28 December for Martin. However, some caveats must be stated: we are mainly concerned with a more realistic representation of the storm from a synoptic perspective. The extreme pressure gradients and their location are therefore considered as important as the value of the minimum. An experiment that does not deepen the minimum but shifts its location in the right direction is therefore considered an improvement (e.g. Fig 9b, where Martin center in the analysis is well-defined, but misplaced one gridpoint to the north). The general tendency of the analyzed center is to lag slightly behind the the observed storm center, because of the extremely high propagation speed. Any dipole pattern that displays the tendency to move the storm in the direction of the propagation, is therefore considered a positive impact. Also, if the experiment experiment produces the same slp minimum of the reference, but sharpening its profile because of increased slp gradients will

be regarded as a positive impact because the storm becomes more confined and thus more intense (and *vice versa*).

Finally, it must be noted that the impact of the various experiments differs between the time of landfall (which is 06 UTC 26 December for Lothar and 1800 UTC 27 December for Martin) where both storms 'appear' in the observations suddenly coming from a data void region, and six hours later when both storms are inland and well depicted by the observing network.

4.2 Detailed impacts

Generally the impact on the analyses of Martin is much stronger than the impact on Lothar. Moreover, the response of fvDAS differs between the two cases, due to the different dynamics of the storms. The following results can be outlined:

Lothar.

Figures 10 and 11 compare pairs of experiments at 0600 UTC and 1200 UTC 26 December. The slp contoured fields represent the reference, and the difference between the experiment and the reference is super-imposed.

- Comparison with the control. At 0600 UTC, EXP2 (Figure 10a), EXP3 (not shown), EXP5 (Figure 10b), EXP7 (not shown) and EXP13 (Figure 10e), when compared to the control (EXP1), produce small or moderate positive impacts, generally with a decrease in the center slp of about 0.5-2.0 hPa, and/or an increase of the surroundings of 0.5-

1.5 hPa, and/or a shift southeast-ward. Particularly, EXP2 and EXP3 can create a closed minimum, which is absent in the control at that time, whereas EXP5, EXP7 and EXP13 shift the storm in the right direction. EXP4, EXP8 and EXP11 produce a negligible impact (not shown), EXP6 (not shown) and EXP9 (Figure 10d) a slightly negative impact (increase in center slp and flattening of the storm).

At 1200 UTC, all the experiments produce a small or moderate positive impact (e.g EXP2, EXP5, EXP7, EXP11 and EXP13 in Figure 10a,b,c,d) except EXP6 (negligible) and EXP9 (small negative impact, not shown). Particularly, EXP5 and EXP7 produce a decrease of the center slp of more than 2 hPa, an increase of the surroundings of more than 1 hPa, causing steeper gradients and a closed minimum (also produced by EXP4, EXP8 and EXP11), placed in the most correct position for the adopted resolution. The best simulation is EXP5, which will be used in the forecast experiments as validating analysis for this specific time.

The anomalies induced in the 900 hPa geopotential field are generally in the range of 5-50 m, and correspond well to the locations where slp anomalies are detected in the corresponding experiments, also for Martin case (not shown).

- Impact of the Eumetsat winds. At 06 UTC 26 December, the usage of EW with default parameters (R=6000 km and K=.6, EXP2) leads to

a positive impact (Figure 10a) with respect to EXP1. However, when the EW are assimilated in EXP3 with $R = 3000\ km$ (thus making the observations more local), the impact on the corresponding experiment (EXP9, having the same $R = 3000\ km$ but with no EW), leads to a better localized storm (Figure 10f). Viceversa, the impact of EW when K=.7 (EXP4-EXP8) is negative (not shown).

At 12UTC, the situation is unchanged for EXP3-EXP9 (positive impact) and EXP4 vs. EXP8 (small negative impact), but there is a stronger positive impact in the EXP2-EXP1 case (Figure 11a).

- Impact of disabling the QuikSCAT thinning. There is a positive impact at 0600 UTC (not shown) and 1200 UTC (Figure 11d), larger in the case of a smaller support (EXP13 vs. EXP9, Figures 10g, 11f).

- Impact of reducing the support R to 3000 km, when Eumetsat winds are assimilated. At both times, 0600 and 1200 UTC, there is a small negative impact if K=.6 (EXP3 vs. EXP2), but a small positive impact either if K=.7 (EXP5 vs. EXP4), or if K=.5 (EXP7 vs. EXP6) (not shown). However, the impacts at K=.5 and K=.7 are different: EXP5 produces pressure changes on the ocean, which propagate also over land, whereas EXP7 produces pressure changes mostly on land. This is consistent with the fact that assimilating EW with K=.7 (EXP5) gives more emphasis to all the observations.

- Impact of reducing the support when Eumetsat winds are not assimilated (EXP9 versus EXP1), with K=.6. This is a case of a slightly negative impact (Figure 10a). In fact, pressure increases at the storm center of about 1.5 hPa at 0600 UTC (Figure 10a) and of about 1 hPa at at 1200 UTC (not shown), flattening the storm.

- Impact of variable K when Eumetsat winds are assimilated The case K=.5 produces a small positive impact (EXP4-EXP2, not shown). The case K=.7 (EXP6-EXP2) is instead another case in which the impact is negative, leading towards a substantial filling of the storm (more than 2hPa), and also to a displacement towards the northwest, in the 'wrong' direction (Figure 10h).

- Impact of variable K when Eumetsat winds are not assimilated Only the case K=.7 is tested (EXP8-EXP1) and the impact is negligible at both times, 0600 and 1200 UTC 26 December.

- Impact of reducing the support when the QuikSCAT thinning is disabled. The impact of smaller support, when denser QuikSCAT data are used (EXP13-EXP11) leads to a small further improvement on the already positive impact of EXP11-EXP1 (not shown).

Martin.

Figures 12 and 13 compare pairs of experiments at 1800 UTC 27 December and 0000 UTC 28 December. The slp contoured field represent the

reference experiment, and the difference between the experiment and the reference is super-imposed. Generally, the impacts are much stronger than in the Lothar case. Note that, as a consequence of the larger impacts, it was necessary to use a larger contour interval in Martin's case.

- Comparison with the control. At 1800 UTC 27 December, all experiments produce generally positive impacts, except EXP6 and EXP8, where the impacts are negligible. There is however an interesting dichotomy: EXP2, EXP3, EXP5, EXP7 shift the storm southward, placing it in the most perfect position for the resolution, but do not deepen it. Conversely, EXP4, EXP9, EXP11 and EXP13 deepen the storm center without shifting it, thus keeping the center at the same position of the control EXP1. Particularly, EXP2-EXP1, EXP3-EXP1 and EXP7-EXP1 (Figures 12a,b,c) reveal the evident bipolar pattern which manifests the tendency of the system to move the storm center in the right direction (cfr. Figure 9b) and also to slightly strengthen the pressure gradients, but without deepening the storm. Conversely, EXP13-EXP1 does not move the storm center but deepens it and also increases substantially the pressure gradient on its western side (Figure 12d). EXP13 provides the lowest center pressure of all experiments and the strongest gradients.

  At 00 UTC 28 December, all experiments produce positive impacts except EXP8 and EXP9, which impact is negligible (not shown). Par-

ticularly, the same bipolar pattern is detected for EXP2-EXP1, EXP3-EXP1, EXP7-EXP1, and some strengthening occurs in EXP13-EXP1 (Figures 13a,b,c,d), although the latter is not as strong as at 1800 UTC 27 December.

- Impact of the Eumetsat winds. At 18 UTC 27 December, the usage of EW with default parameters (R=6000 km and K=.6) is conducive, as seen, to a very positive impact (Figure 12a). A positive impact is also present when the EW are assimilated with R=3000 (EXP3-EXP9) (Figure 12e). There is virtually no impact when EW are assimilated at K=.7 (EXP4-EXP8, not shown). At 00UTC, the situation is the same (not shown).

- Impact of disabling the QuikSCAT thinning. There is a positive impact at 1800 UTC 27 December (not shown), where the lowest analyzed slp center value is produced (although not as accurately placed as EXP2) and at 0000 UTC 28 December, for both cases of R=6000 (EXP11-EXP1, not shown) and R=3000 (EXP13-EXP9, Figure 13e).

- Impact of reducing the support R to 3000 km, when Eumetsat winds are assimilated. At both times, 1800 27 December and 0000 UTC 28 December, there is an overall positive impact if K=.6 (EXP3 vs. EXP2,), if K=.7 (EXP5 vs. EXP4), and if K=.5 (EXP7 vs. EXP6). We select to plot EXP3-EXP2 at 1800 UTC 27 December (Figure 12f),

that deepens the storm and strongly increases the gradients, and EXP7-EXP6 at 0000 28 December (Figure 13f, where beyond deepening and increased gradients there is also a tendency to shift the center correctly (eastward).

- Impact of reducing the support when Eumetsat winds are not assimilated (EXP9 versus EXP1), with K=.6. This is a case of a negligible to slightly-negative impact (not shown). The storm gets slightly strengthened but is also displaced in the wrong direction at both times.

- Impact of variable K when Eumetsat winds are assimilated. At both times, all cases produce a strengthening of storms and gradients, but without improving its position or slightly worsening it with respect to EXP2 (thus returning towards the control position, that EXP2 improves). Figures 12g,h and 13g,h display the two cases at 1800 UTC 27 and 00 UTC 28 December.

- Impact of variable K when Eumetsat winds are not assimilated. Only the case K=.7 is tested (EXP8-EXP1) and the impact is virtually zero at both times (not shown).

- Impact of reducing the support when the QuikSCAT thinning is disabled. The impact of smaller support, when denser QuikSCAT data are used (EXP13-EXP11) leads to virtually no impact at both times (not shown).

4.3 Forecast

Figure 14 shows the forecast performed at various short-ranges with the EXP1 settings. The analyses used for comparison are from EXP2 and EXP5 at 0600 26 December and 1200 UTC December (Figure 14): the former is not adequate for the intensity but only for the position, the latter is a decent representation of the storm (recall slp observations in Figure 8a,c). Leutbecher et al (2002) point out that Lothar was poorly predicted by operational models in the short-range of 1-3 days, even if these predicted the storms quite well at the 4-5 day range. The fvDAS is affected by this problem to a lesser extent.

In fact, in Figure 14a,b, the forecasts initialized at 1200 UTC 23 December for a verification at 06 UTC 26 December (66 hour forecast) and 1200 UTC 26 December (72 hour forecast) are displayed. The storm is extremely deep (961 hPa) at 0600 UTC, and its scale is very well represented. However, its location is slightly incorrect in both cases, as the comparison with the analyses reveal.

Moving close to the time of the verifying analyses (initialization at 1200 UTC 24 December), the performance deteriorates (Figure 14c,d), but there is still a substantially deep low at both times. The final simulation (initialization at 1200 UTC 25 December) is subject to a further deterioration, but the predicted position is very accurate (Figure 14e,f).

The most interesting result is obtained when assimilating EW or disabling

the QW thinning with different K and support. Surprisingly, most of these forecast deteriorate the performance of the model. The only exceptions are EXP13 (simulation with full-density QW and R=3000) and EXP2, which assimilates EW. The first setting performs well in the forecast for 1200 UTC 26 Dec from 72 and 24 hours (Figures 15a,b): the intensity and the position are quite well represented.

The best result is the 24 hour forecast obtained by assimilating the Eumetsat winds: a 965 hPa minimum is obtained, in a very accurate position (Figure 15c).

5 Interpretation of results

5.1 Summary of results

The experiments performed lead to the following overall conclusions: Lothar is relatively easy to predict at the medium range, more difficult to predict at the shorter range, and its analysis is extremely unsatisfactory. It is found that the analysis can be slightly improved at the landfall time (0600 UTC) by assimilating high resolution Meteosat winds. The analyzed storm can be deepened more substantially when it is already inland (at 1200 UTC) by assimilating Meteosat winds with narrower background error correlation (thus making observation impacts more localized) and with a higher gain, that is, increasing the overall weight of the observations.

For Martin, we find that the analysis is quite satisfactory at the time of

landfall (1800 UTC 27 December), and it can be further deepened by: (1) reducing the support, (2) assimilating Eumetsat winds at R=6000 but with K=.7, thus increasing the overall weight of observations, (3) assimilating full-density QuikSCAT winds at any support. The storm can also be moved to the right position, without deepening, by: (1) assimilating the Eumetsat winds with the default parameters (K=.6, R=6000), (2) assimilating the Eumetsat winds at any K but with R=3000 support. The analysis of Martin is quite good when the storm is inland, but the impact of additional data sets is still generally positive.

It is found that Lothar is predicted very well by the fvDAS system, with the default settings used for the control run (EXP1), even at the short range (1 to 3 days). Additional data sets or modifications generally worsen the forecast, except when assimilating QuikSCAT with reduced support (for forecast shorter than 3 days), and Eumetsat (exclusively at the 1-day range). The latter improves the forecast tremendously. Finally, it is found that we are unable to generate a satisfactory numerical forecast of Martin at *any* range.

5.2 Dynamic considerations

In order to understand the underlying differences in the dynamics of the storms, we show in Figure 16 a sequence of meridional cross-sections of wind and temperature across the center of Lothar at three different stages of the evolution (0600, 1200 UTC 25 December and 0000 UTC 26 December). The sections are taken at different longitudes, because of the high propagation

speed. Lothar can be identified by the low-level wind maximum also evident in the 900 hPa wind (recall Figure 2). Once Lothar is situated directly below the upper-level jet, at 0000 UTC 26 December, as shown by Wernli et al. (2002) there is a sudden release of baroclinic instability and the explosive development occurs. The cross-section shows very strong vertical shear at approximately $48^{o}N$ where the storm is located at this time, and the drop of about 200 hPa in all the isotherms on the storm-scale confirm the scenario. So, the dynamics of Lothar appear in large part driven by the upper-level jet, as stated also by these authors, and are unquestionably extremely baroclinic.

The case of Martin is quite different. Recalling Figure 3, a low-level jet, parallel to the upper-level jet stream, corresponding to Martin, can be seen. This jet has an interesting vertical structure. In Figures 17 and 18, one can see vertical cross-sections across the center of Martin, as it moves across the Atlantic from 0600 UTC 25 December (at $38^{o}W$) to 1200 UTC 27 December (at $8^{o}W$), shortly before landfall. The striking aspects are:

- A dramatic increase of kinetic energy of the low-level jet, the maximum speed of which increases from 26 $m\,s^{-1}$ to more than 50 $m\,s^{-1}$.
- A decrease of kinetic energy of the upper-level jet, which speed decreases from 94 $m\,s^{-1}$ to 74 $m\,s^{-1}$ (disappearing at the time in which Martin develops).
- A gradual alignment of the low-level and the upper-level jets, which

end up creating, at 1200 UTC, a vertical column from 900 to 300 hPa in which there is a horizontal shear of 3f, and essentially no vertical shear (Figure 18c).

The difference between the two storms at the time shortly before landfall is evident. These findings have two possible implications: (1) the low-level jet might be responsible for stabilizing the upper-level jet, until it remains in the right entrance region. In fact, the transversal circulation induced by the low-level jet exit region contrasts the transversal circulation induced at the entrance region of the upper-level jet, acting in the opposite way of a normal jet-coupling (e.g. Uccellini et al. 1987). Moreover, the low-level jet creates *negative* vertical shear above it, thus neutralizing the baroclinicity of the upper-level jet in the low-levels (e.g. Fig 17c). This would explain why the upper-level jet could retain its straight structure for so long. (2) Once the low-level jet becomes aligned with the upper-level jet, a large amount of energy becomes available for barotropic instability caused by horizontal shear (Figure 17d).

In a linear theory framework, the necessary condition for barotropic instability to occur in a zonal flow varying with latitude and time $U(y,t)$, with no vertical shear (i.e., in a barotropic atmosphere) and a nonzero meridional velocity shear $\frac{\partial U}{\partial y}$, symmetrical with respect of a certain latitude, is (Kuo 1949):

$$\beta - \frac{\partial^2 U}{\partial y^2} = 0 \qquad (2)$$

Nitta and Yanai (1969) studied the barotropic instability of two profiles of a westerly and an easterly jet and concluded (by calculating a family of critical curves, which provides the growth rate for a wave of wavelength L, extracting energy from a jet of given intensity and width) that barotropic instability appears to develop more easily on the southern flank of an easterly jet. Based on these results, it has been generally agreed that horizontal shear, and therefore barotropic instability, cannot be considered the main cause for the development of cyclones located poleward of a westerly jet. The main reason is that it was believed that westerly jets do not become narrow enough to develop horizontal shears adequate to trigger unstable wavelengths of the size typical of polar lows or explosive cyclones. Sardie and Warner (1985) and Businger and Reed (1989) concluded that, given what was considered a 'strong' shear for a westerly jet (i.e, 80 $m\,s^{-1}$ over 500 km), the corresponding growth rate would be too small for any substantial development.

The case studied here reveals a horizontal shear of at least twice this value, and provides some evidence of a mechanism of interaction between a low-level and upper-level jet that could partly explain the dynamics of Martin via barotropic instability. There is a number of recent studies in which the contribution of barotropic instability to the development of cyclones located poleward of a westerly jet is reconsidered, either theoretically (e.g. Kucharsky and Thorpe 2001) or observationally (e.g. Reale and Atlas 2001). These and other studies refer to very different situations; however, one important fact

is that contemporary denser and higher quality data-sets, like the EW for example, reveal the fine velocity structure in the flanks of the jet, confirming the occasional presence of horizontal shears much stronger than the ones which were considered as 'strong' in the '80s. Therefore, the possibility of an important cyclogenetic role played by the barotropic instability of westerly jets cannot be dismissed.

If we accept this intrinsic difference in the dynamics of Lothar and Martin, some of the perplexing aspects found in our experiments can be explained. Lothar is driven predominantly by the upper-level jet, and as such the information provided by the Eumetsat winds is very significant on the shorter time-scale. In fact, in Figure 19, the information provided by Eumetsat at 1200 UTC 25 December is shown. There is a clear fine-structure, namely a small-scale jet streak with substantial acceleration, between longitudes 6^oW and 3^oE at about 48^oN: the wind increases from 130 kt to 150 kt, well ahead of the main speed maximum which is still to the west, out of the domain of the plot (recall Figure 2). This small-scale secondary maximum detected by the EW, is not captured in the control analyses and it is responsible for a dramatic increase in upper-level divergence. It is likely that the assimilation of EW leads to an overall better performance in the analyses and in the 1-day forecast because this structure is captured in the system (recall the excellent forecast initialized at 1200 UTC 25 December, Figure 15c). QW can also improve the forecast, since these data obviously provide surface wind infor-

mation around the developing cyclone, but it is not as effective as the EW in the 1-day range.

Conversely, Martin is driven by a cooperation between the upper-level and the lower-level jet. The impact of both QW and EW is therefore strong in the analyses. However, even these data are not sufficient to make a good forecast because of the inability of the model to retain the aligned configuration without releasing instability. Most of the experiments develop the instability too early, leading to one or more cyclones much weaker than Martin, because the instability available in Figure 18c is not being used efficiently. The extreme horizontal shears visible in the cross-sections in Figure 18, are generally poorly captured in the forecasts (not shown). It seems that the transition between 1800 UTC 26 December and 1200 UTC 27 December would require wind observations between 700 hPa and 500 hPa, something that neither QW nor EW can provide.

6 Conclusions

In this work the two storms that affected France and most of central Europe between 26 and 28 December 1999 are studied. A set of data assimilation experiments, using the finite volume Data Assimilation System developed at the Data Assimilation Office of the NASA Goddard Space Flight Center, are performed. The main goal is to produce better analyses and forecast for these two events, by using two additional data sets, Eumetsat and QuikSCAT

winds, and by perturbing the way they are being assimilated.

It is found that the two storms, in spite of their proximity and intensity, are captured differently by the data assimilation system. The first storm appears to be well predicted by the system, but difficult to analyze. We improve the analyses by assimilating Eumetsat winds and by reducing the support and the weight of the information. The second storm appears to be analyzed well by the system, but no substantial improvement to the forecast resulted from any experiment. This is possibly due to a critical data void in the region between 700 and 500 hPa where part of the storm development seems to take place.

Acknowledgments This work was supported by grants GEST-910-00-012 and GEST-910-01-010. Thanks are due to Dr. Meta E. Sienkiewicz for her valuable help in several of the experiments and to Dr. Greg Gaspari for helping in implementing the covariance model in the version of fvDAS we used.

REFERENCES

Businger, S. and R. J. Reed, 1989: Cyclogenesis in Cold Air Masses, *Wea. Forecasting,* **4,** 133-156.

Gaspari, G. and S. Cohn, 1999: Construction of correlation functions in two and three dimentions. *Q. J. R. Meteorol. Soc.,* **125,** 723-757.

Hello, G. and F. Lalaurette and J.-N. Thepaut, 2000: Combined use of sensitivity information and observations to improve meteorological forecasts: A feasibility study applied to the 'Christmas storm' case. *Q. J. R. Meteorol. Soc.,* **126,** 621-647.

Kucharsky, F. and A. J. Thorpe, 2001: The influence of transient upper-level barotropic growth on the development of baroclinic waves. *Q. J. R. Meteorol. Soc.,* **127,** 835-844.

Kuo, H. L., 1949: Dynamic instability of two-dimensional non-divergent flow in a barotropic atmosphere. *J. Meteor.,* **6,** 105-122.

Leutbecher, J. Barkmeijer, T. N. Palmer and A. J. Thorpe, 2002: Potential improvements of forecasts of two severe storms using targeted observations. *Q. J. R. Meteorol. Soc.,* 105-122.

Lin, S. J. and R. Rood, 1996: Multidimensional Flux-Form Semi-Lagrangian Transport Schemes *Mon. Wea. Rev.*, **124,** 2046-2070.

Nitta, T. and M. Yanai, 1969: A note on the barotropic instability of the tropical easterly current. *J. Meteor. Soc. Japan.* **47,** 127-130.

Reale, O. and R. Atlas 2001: Tropical Cyclone-like Vortices in the Extratropics: Observational Evidence and Synoptic Analysis. *Wea. Forecasting*, **16,** 7-34.

Sardie, J. M. and T. T. Warner, 1983: On the mechanism for the devlopment of polar lows. *J. Atmos. Sci.*, **40,** 869-881.

Sardie, J. M. and T. T. Warner, 1985: A numerical study of the development mechanism of polar lows. *Tellus*, **37,** 869-881.

Uccellini, L.W., R. A. Petersen, K. F. Brill, P. J. Kocin and J. J. Tuccillo, 1987: Synergistic interactions between an upper-level jet streak and diabatic processes that influence the development of a low-level jet and a secondary coastal cyclone. *Mon. Wea. Rev.*, **115,** 2227-2261.

Ulbrich, U., A. H. Fink, M. Klawa and J. G. Pinto, 2001: Three extreme storms over Europe in December 1999 *Weather*, **56,** 70-80.

Wernli, H., S. Dirren, M. Liniger and M. Zillig, 2002: Dynamical aspects of the life of the winter storm 'Lothar' (24-26 December 1999). *Q. J. R. Meteorol. Soc.*, **128,** 405-429.

Table Caption

Table 1. Experiments. The first column shows the value of K, defined as $\sigma^2_{Forecast}/(\sigma^2_{Forecast} + \sigma^2_{Observations})$. The second column shows the value of R, correlation function support, in km. The third column refers to the assimilation of the full-density QuikSCAT data: Y indicates that the thinning is disabled, thus making usage of full-resolution QuikSCAT data; N indicates that the thinning is enabled, so only a subset of QuikSCAT data is being used. The fourth column refers to the usage of the High Resolution Meteosat Winds.

	K	R	HR Qscat	HR Meteosat
EXP 1 (Control)	0.6	6000	N	N
EXP 2	0.6	6000	N	Y
EXP 3	0.6	3000	N	Y
EXP 4	0.7	6000	N	Y
EXP 5	0.7	3000	N	Y
EXP 6	0.5	6000	N	Y
EXP 7	0.5	3000	N	Y
EXP 8	0.7	6000	N	N
EXP 9	0.6	3000	N	N
EXP 11	0.6	6000	Y	N
EXP 13	0.6	3000	Y	N

Table 1: Experiments. The first column shows the value of K, defined as $\sigma^2_{Forecast}/(\sigma^2_{Forecast} + \sigma^2_{Observations})$. The second column shows the value of R, correlation function support, in km. The third column refers to the assimilation of the full-density QuikSCAT data: Y indicates that the thinning is disabled, thus making usage of full-resolution QuikSCAT data; N indicates that the thinning is enabled, so only a subset of QuikSCAT data is being used. The fourth column refers to the usage of the High Resolution Meteosat Winds.

Figure 1: Sea level pressure (hPa, continuous line), 900 hPa wind speed (dashed line, contours at $20, 40\ m\,s^{-1}$) and 300 hPa wind speed (shaded, values at $60, 70, 80, 90 m\,s^{-1}$) at 12 UTC 21 December 1999 (a), 12 UTC 22 December 1999 (b), at 12 UTC 23 December 1999 (c), 12 UTC 24 December 1999 (d).

Figure 2: Sea level pressure (hPa, continuous line), 900 hPa wind speed (dashed line, contours at $20, 30, 40\ m\,s^{-1}$) and 300 hPa wind speed (shaded, values at $60, 70, 80, 90 m\,s^{-1}$) at 0000 UTC 25 December 1999 (top), 1200 UTC 25 December (center) and 0000 UTC 26 December 1999 (bottom).

Figure 3: Sea level pressure (hPa, continuous line), 900 hPa wind speed (dashed line, contours at $20, 30, 40\ m\,s^{-1}$) and 300 hPa wind speed (shaded, values at $60, 70, 80, 90\ m\,s^{-1}$) at 1200 UTC 26 December 1999 (top), 0000 UTC 27 December (center) and 1200 UTC 27 December 1999 (bottom).

Figure 4: Sea level pressure (hPa, left panels), and 500 hPa geopotential height (m, right panels) at at 0600 UTC 25 December 1999 (a, b), 1200 UTC 25 December (c, d), 1800 UTC 25 December (e, f) and 0000 UTC 26 December 1999 (g, h).

Figure 5: Sea level pressure (hPa, left panels), and 500 hPa geopotential height (m, right panels) at at 0600 UTC 26 December 1999 (a, b), 1200 UTC 26 December (c, d), 1800 UTC 26 December (e, f) and 0000 UTC 27 December 1999 (g, h).

Figure 6: Sea level pressure (hPa, left panels), and 500 hPa geopotential height (m, right panels) at at 0600 UTC 27 December 1999 (a, b), 1200 UTC 27 December (c, d), 1800 UTC 27 December (e, f) and 0000 UTC 28 December 1999 (g, h).

Figure 7: NOAA polar satellite images in the infrared bandwidth, channel 4. Courtesy of Dundee Satellite Receiving Station, Dundee University, Scotland. The center of Lothar can be identified with a dense cirrus shield located on the Channel at 04:37 (a); the center of Martin corresponds to a low-level vortex over northwestern France at 19:01 27 December 1999 (b).

Figure 8: Storm Lothar. Sea level pressure observations (a) and automated analysis of sea level pressure (contour) with observed (digits) 6-hourly change (b) at 0600 UTC 26 December 1999. Sea level pressure observations (c) and automated analysis of sea level pressure (d) at 1200 UTC 26 December 1999. The 'true' position of the center, estimated from surface observations, is marked with 'L' in all four plots.

Figure 9: Storm Martin. Sea level pressure observations (a) and automated analysis of sea level pressure (contour) with observed (digits) 6-hourly change (b) at 1800 UTC 27 December 1999. Sea level pressure observations (c) and automated analysis of sea level pressure (d) at 0000 UTC 28 December 1999. The 'true' position of the center, estimated from surface observations, is marked with 'M' in all four plots.

Figure 10: Assimilation experiment results for Lothar at 0600 UTC 26 December 1999. Sea level pressure (contour interval 2hPa) analyses for the reference experiments EXP1 (a,b,c,d,e,), EXP9 (f,g) and EXP2 (h). Departure from reference EXP2-EXP1 (a), EXP5-EXP1 (b), EXP7-EXP1 (c), EXP9-EXP1 (d), EXP13-EXP1 (e), EXP3-EXP9 (f), EXP13-EXP9 (g) and EXP6-EXP2 (h) are super-imposed. Dark/light shaded areas represent areas where slp increases/decreases more than +/-0.5 hPa. Contours are added at +/- 1, 1.5, 2, 2.5 hPa.

Figure 11: Assimilation experiment results for Lothar at 1200 UTC 26 December 1999. Sea level pressure (contour interval 2hPa) analyses for the reference experiments EXP1 (a,b,c,d,e,), EXP9 (f,g) and EXP2 (h). Departure from reference EXP2-EXP1 (a), EXP5-EXP1 (b), EXP7-EXP1 (c), EXP11-EXP1 (d), EXP13-EXP1 (e), EXP3-EXP9 (f), EXP13-EXP9 (g) and EXP6-EXP2 (h) are super-imposed. Dark/light shaded areas represent areas where slp increases/decreases more than +/-0.5 hPa. Contours are added at +/- 1, 1.5, 2, 2.5 hPa.

Figure 12: Assimilation experiment results for Martin at 1800 UTC 27 December 1999. Sea level pressure (contour interval 2hPa) analyses for the reference experiments EXP1 (a,b,c,d), EXP9 (e) and EXP2 (f,g,h). Departure from reference EXP2-EXP1 (a), EXP3-EXP1 (b), EXP7-EXP1 (c), EXP13-EXP1 (d), EXP3-EXP9 (e), EXP3-EXP2 (f), EXP4-EXP2 (g) and EXP6-EXP2 (h) are super-imposed. Dark/light shaded areas represent areas where slp increases/decreases more than +/-0.5 hPa. Contours are added at +/- 1, 2, 3, 4, 5 hPa. Note the different contour interval for the anomalies, with respect to Figures 10 and 11.

Figure 13: Assimilation experiment results for Martin at 0000 UTC 28 December 1999. Sea level pressure (contour interval 2hPa) analyses for the reference experiments EXP1 (a,b,c,d), EXP9 (e), EXP6 (f) and EXP2 (g,h). Departure from reference EXP2-EXP1 (a), EXP3-EXP1 (b), EXP7-EXP1 (c), EXP13-EXP1 (d), EXP13-EXP9 (e), EXP7-EXP6 (f), EXP4-EXP2 (g) and EXP6-EXP2 (h) are super-imposed. Dark/light shaded areas represent areas where slp increases/decreases more than +/-0.5 hPa. Contours are added at +/- 1, 2, 3, 4, 5 hPa. Note the different contour interval for the anomalies, with respect to Figures 10 and 11.

Figure 14: Forecast experiment results, relative to the EXP1 specifics, for Lothar at 0600 UTC (left panels) and 1200 UTC 26 December (right panels). Forecast initialized at 1200 UTC 23 December (a,b), at 1200 24 December (c,d), at 1200 UTC 25 December (e,f) and 'best' analyses from EXP2 (g) and EXP5 (h).

Figure 15: Forecast experiment results, relative to the EXP13 (a, b) and EXP2 (c) specfics, for Lothar at 1200 UTC 26 December. Forecast initialized at 1200 UTC 23 December (a), at 1200 UTC 25 December (b, c).

Figure 16: Meridional cross-sections of wind ($m\,s^{-1}$ and temperature (^oC) across the storm Lothar at 0600 UTC 25 December and 38^oW (left), at 1200 UTC 25 December and 28^oW (center), and at 0000 UTC 26 December and 8^oW (right).

Figure 17: Meridional cross-sections of wind ($m\,s^{-1}$ and temperature (^oC) across the storm Martin at 1200 UTC 25 December and 54^oW (left), at 1800 UTC 25 December and 50^oW (center), and at 0000 UTC 26 December and 45^oW (right).

Figure 18: Meridional cross-sections of wind ($m\,s^{-1}$) and temperature (^oC) across the storm Martin at 1800 UTC 26 December and 35^oW (left), at 0000 UTC 27 December and 26^oW (center), and at 1200 UTC 27 December and 8^oW (right).

Figure 19: Eumetsat wind at 1800 UTC 25 December. The digits represent the pressure level at which the observation is attributed.

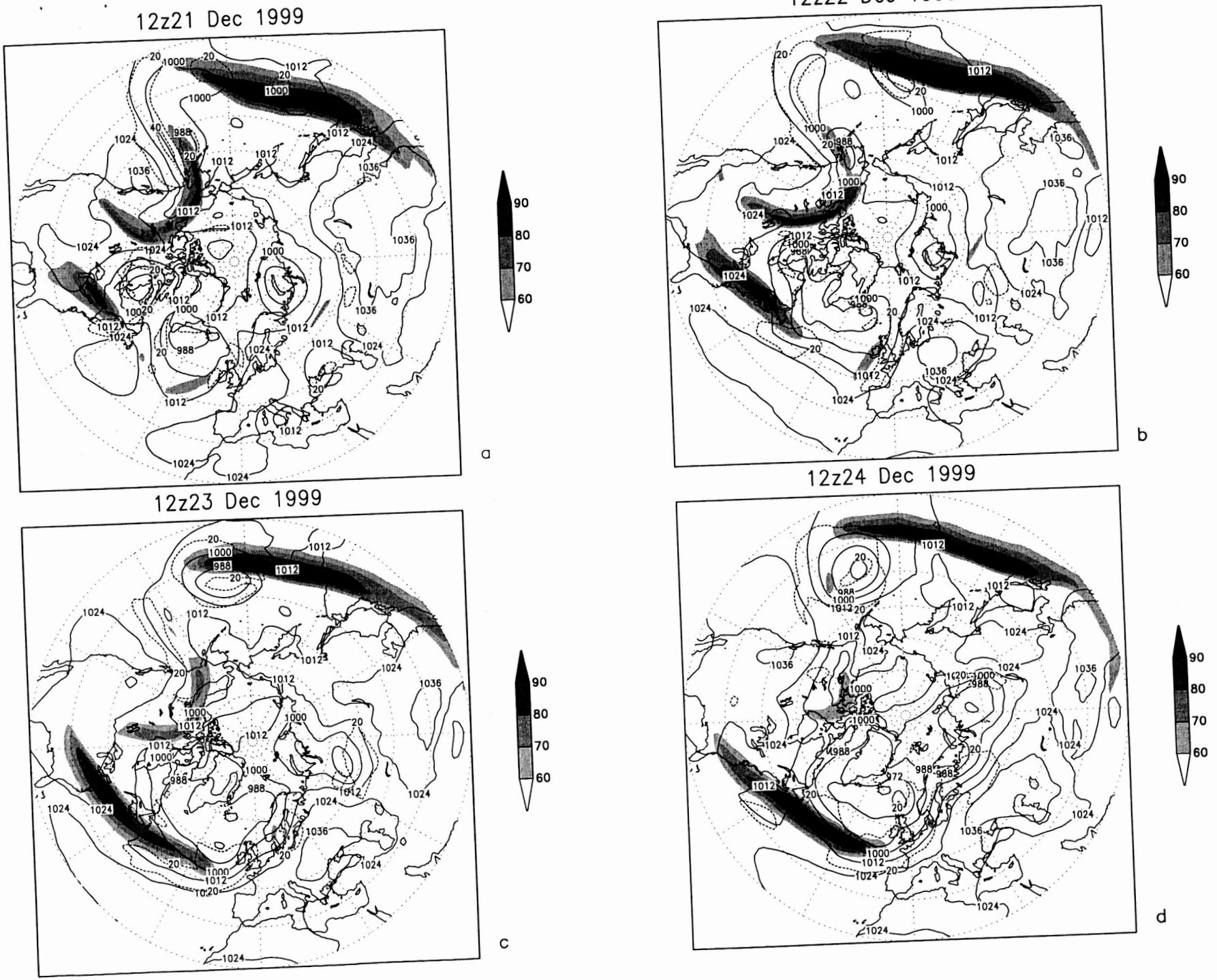
12z21 Dec 1999
12z22 Dec 1999
12z23 Dec 1999
12z24 Dec 1999
90
80
70
60
a
b
c
d

Fig 1

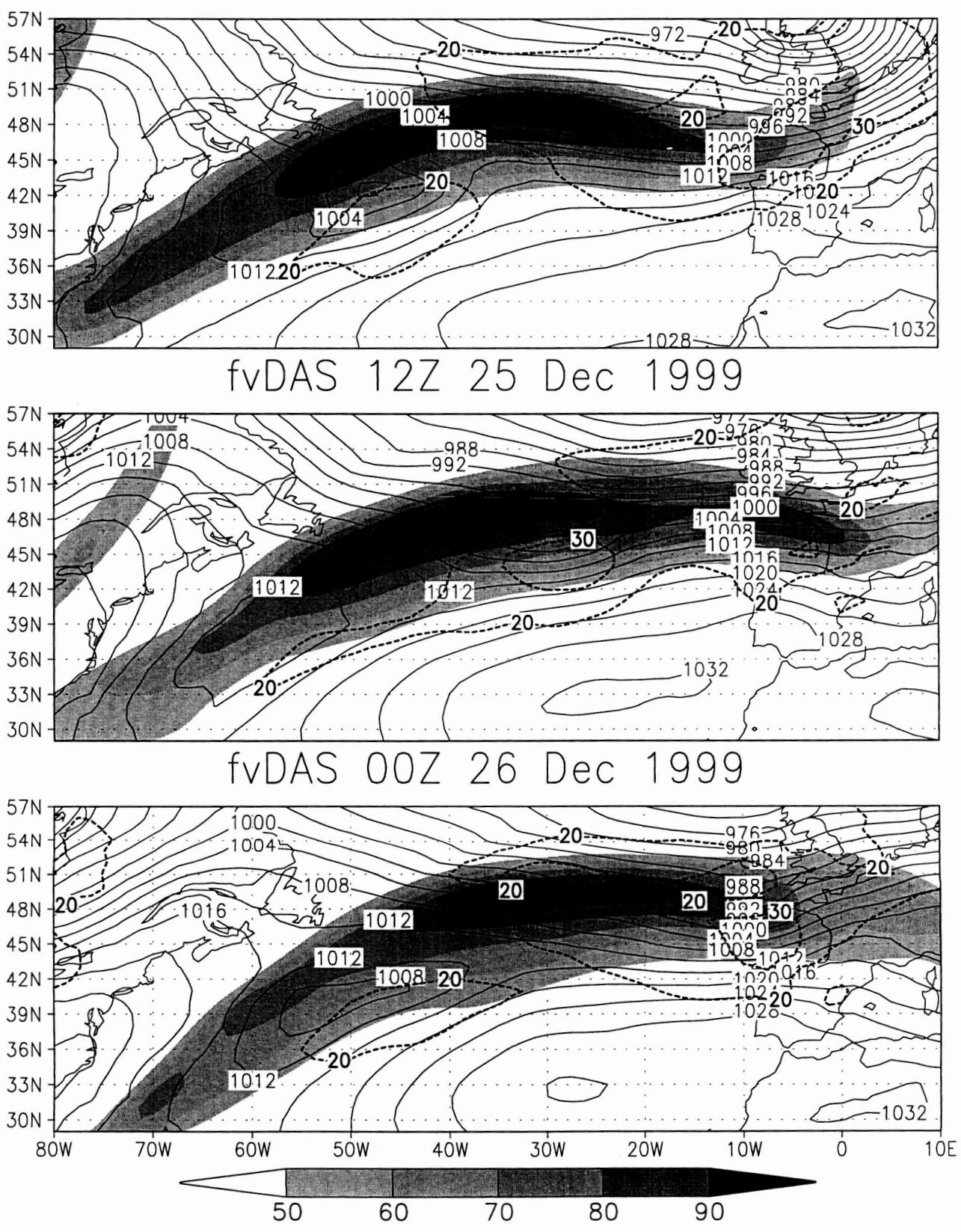
fvDAS 00Z 25 Dec 1999
fvDAS 12Z 25 Dec 1999
fvDAS 00Z 26 Dec 1999
57N
54N
51N
48N
45N
42N
39N
36N
33N
30N
80W
70W
60W
50W
40W
30W
20W
10W
0
10E
50
60
70
80
90

Fig 2

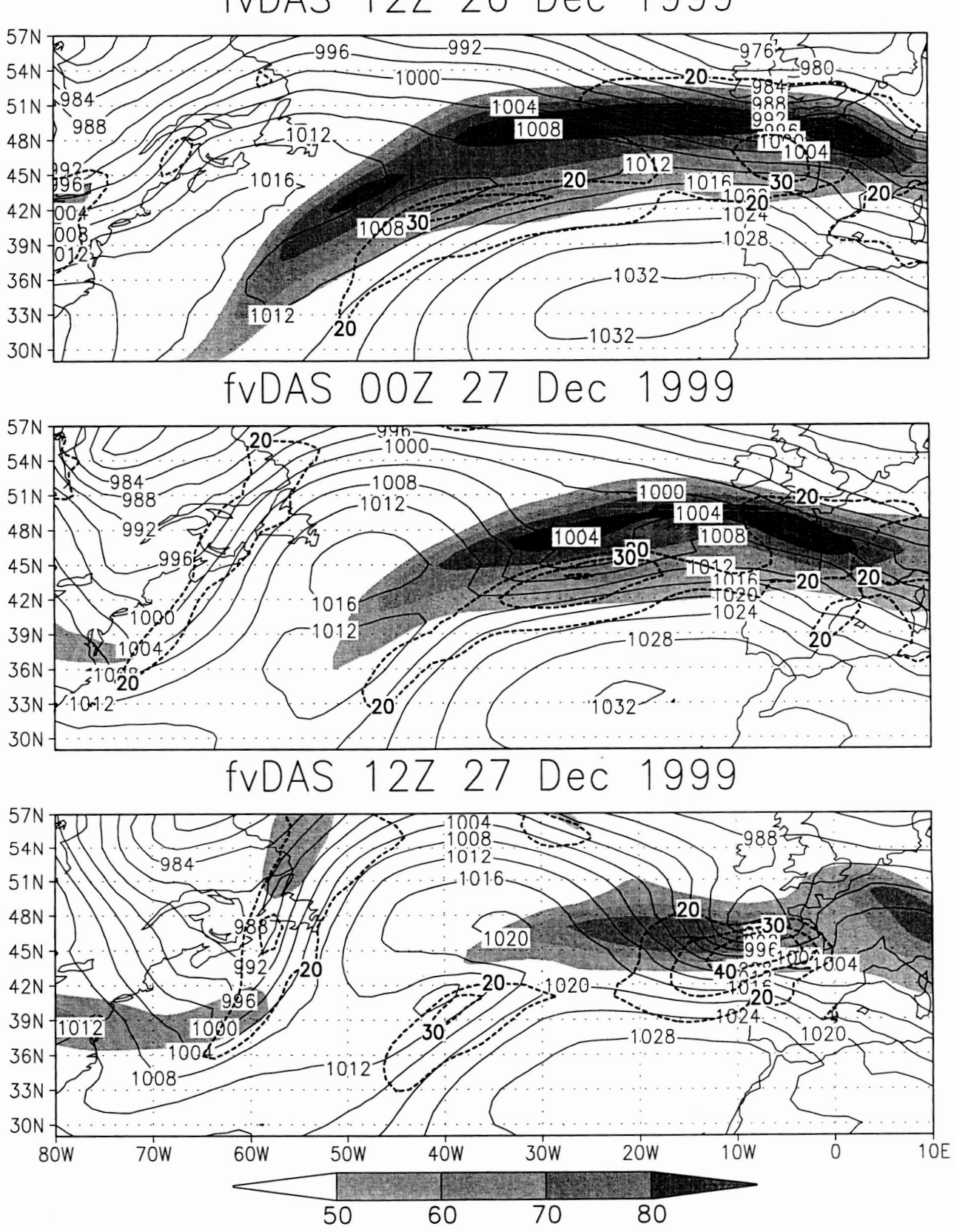
fvDAS 12Z 26 Dec 1999
fvDAS 00Z 27 Dec 1999
fvDAS 12Z 27 Dec 1999
57N
54N
51N
48N
45N
42N
39N
36N
33N
30N
80W
70W
60W
50W
40W
30W
20W
10W
0
10E
50
60
70
80

Fig 3

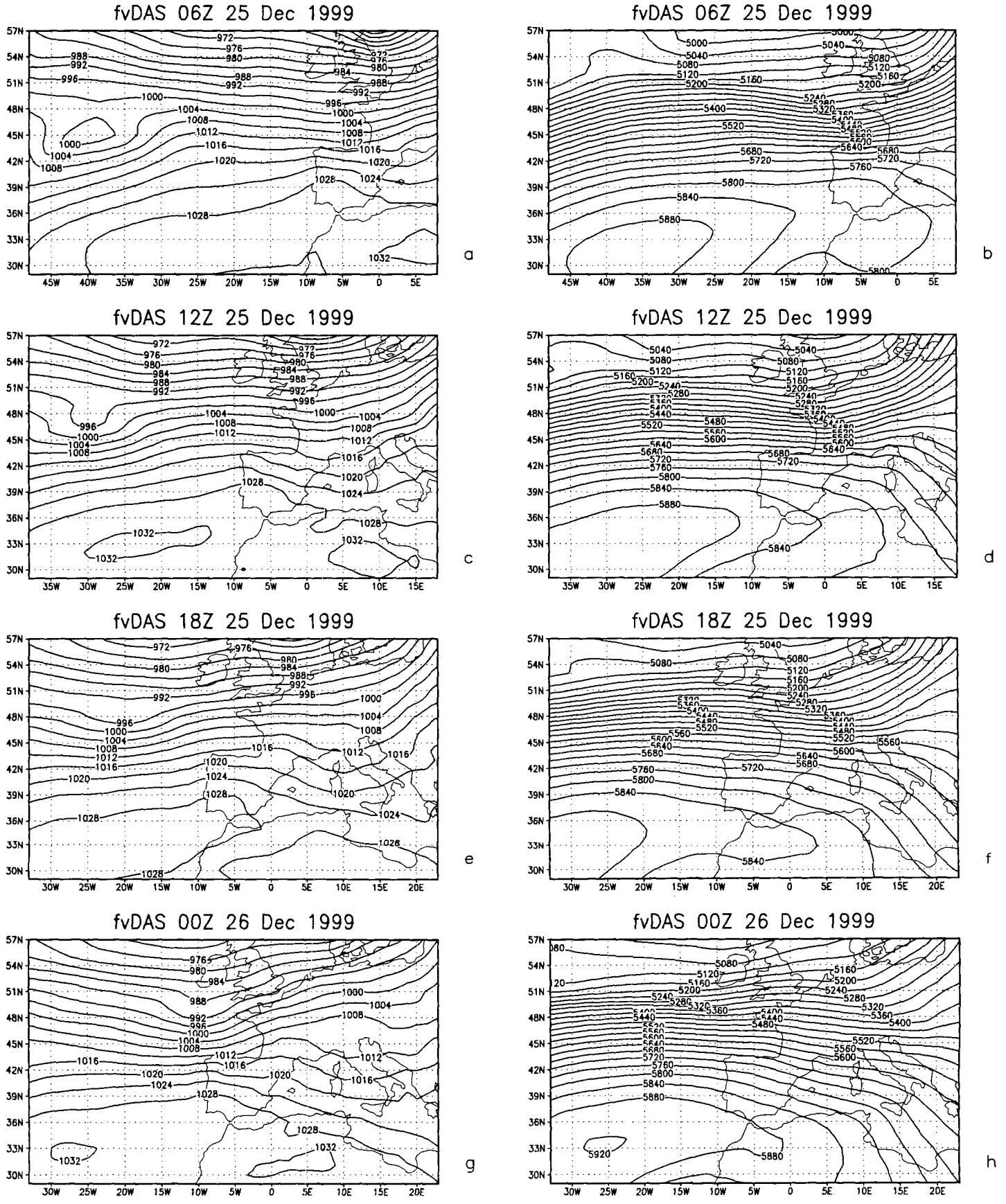
fvDAS 06Z 25 Dec 1999
a
fvDAS 06Z 25 Dec 1999
b
fvDAS 12Z 25 Dec 1999
c
fvDAS 12Z 25 Dec 1999
d
fvDAS 18Z 25 Dec 1999
e
fvDAS 18Z 25 Dec 1999
f
fvDAS 00Z 26 Dec 1999
g
fvDAS 00Z 26 Dec 1999
h

Fig 4

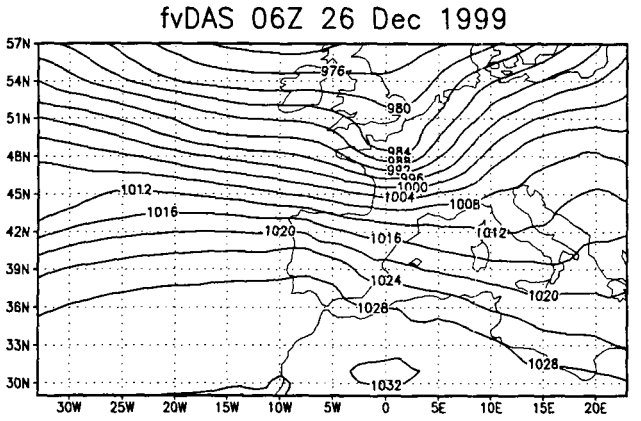
fvDAS 06Z 26 Dec 1999

a

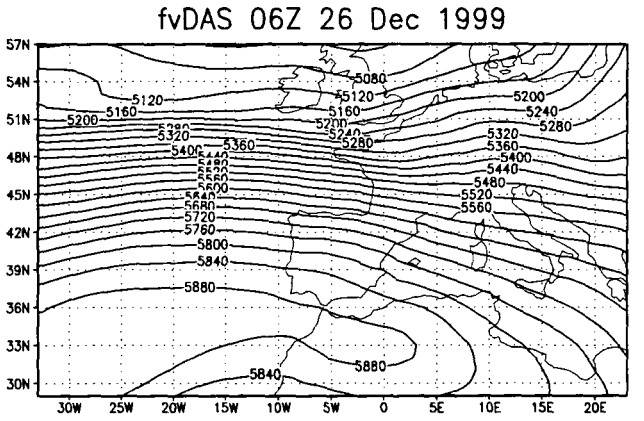
fvDAS 06Z 26 Dec 1999

b

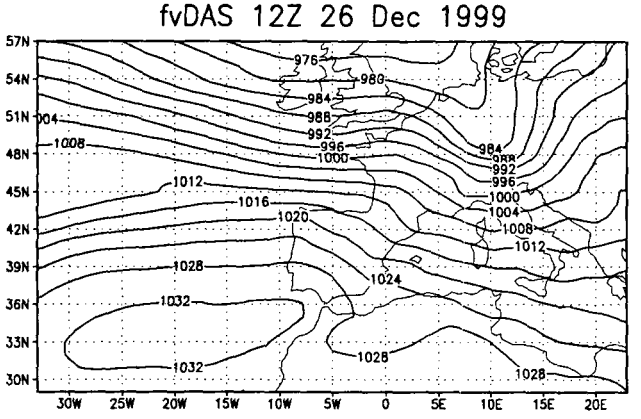
fvDAS 12Z 26 Dec 1999

c

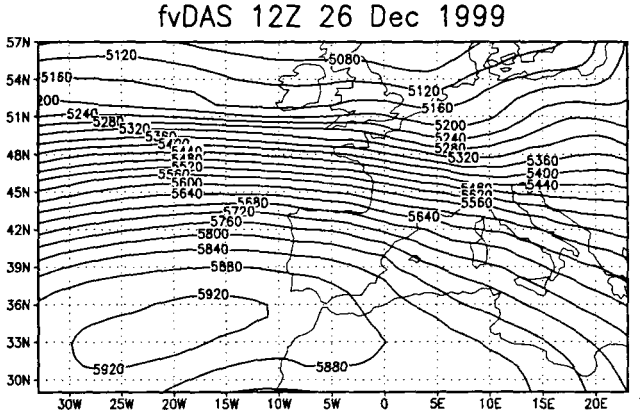
fvDAS 12Z 26 Dec 1999

d

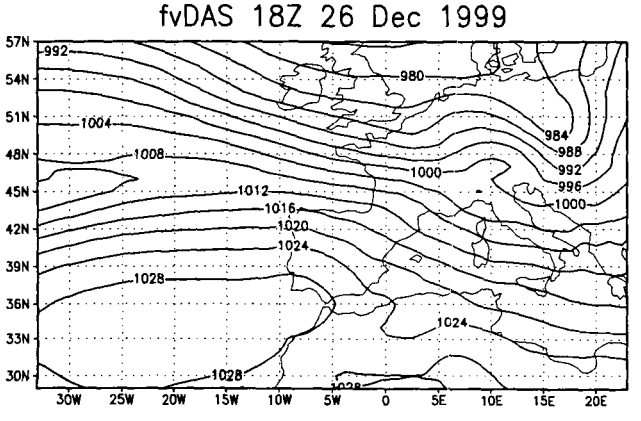
fvDAS 18Z 26 Dec 1999

e

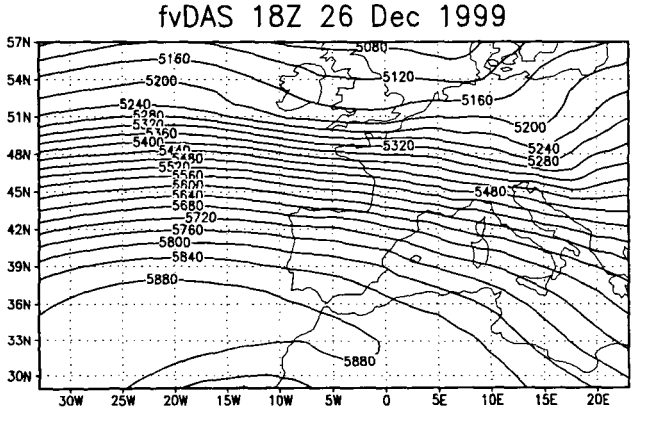
fvDAS 18Z 26 Dec 1999

f

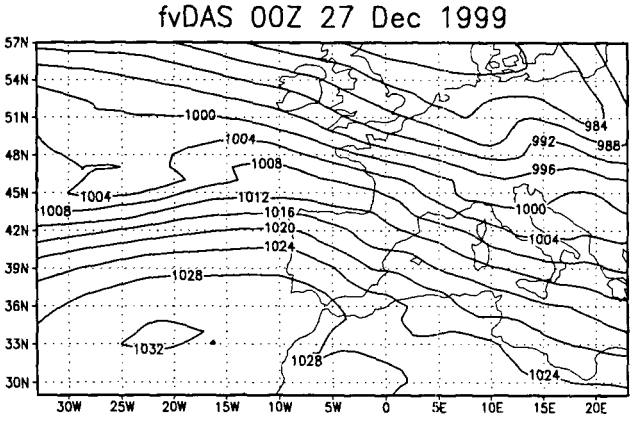
fvDAS 00Z 27 Dec 1999

g

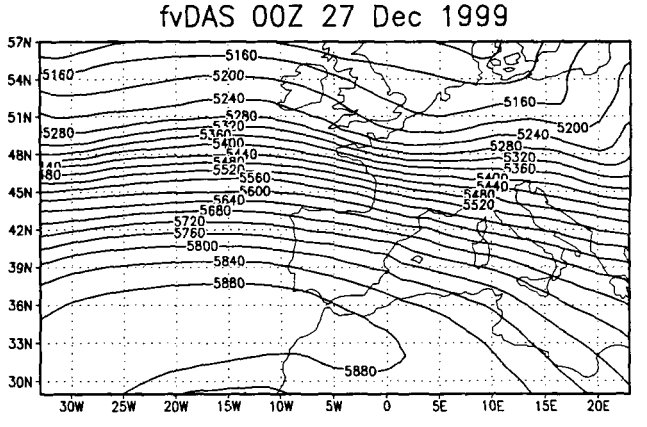
fvDAS 00Z 27 Dec 1999

h

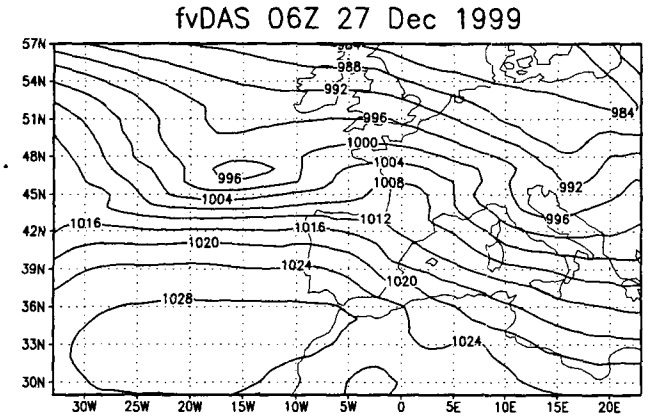

a

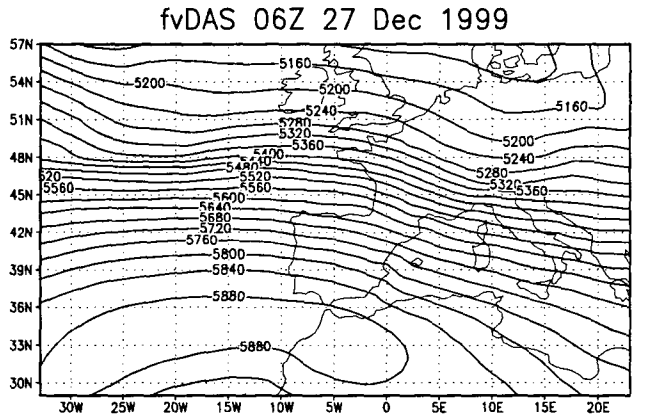

b

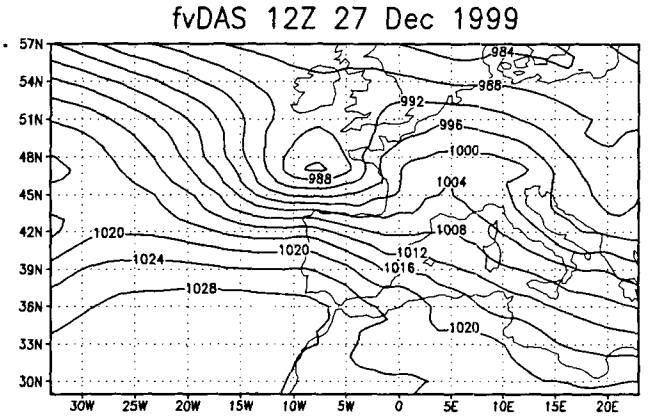

c

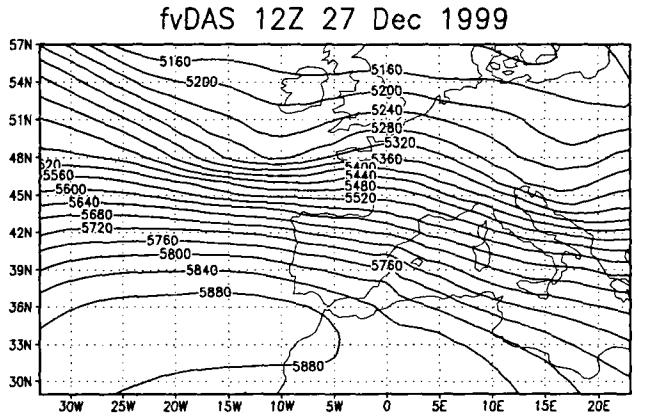

d

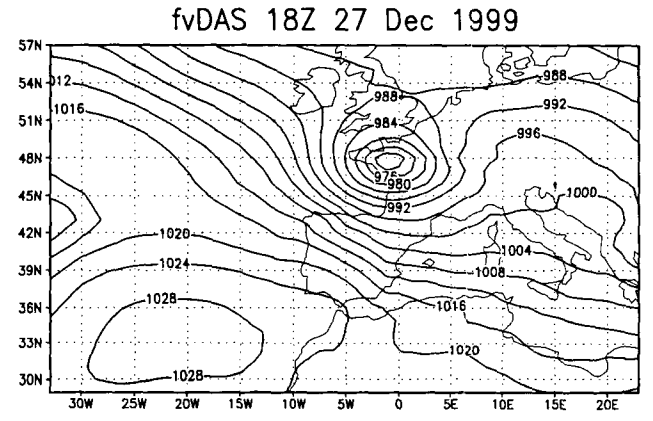

e

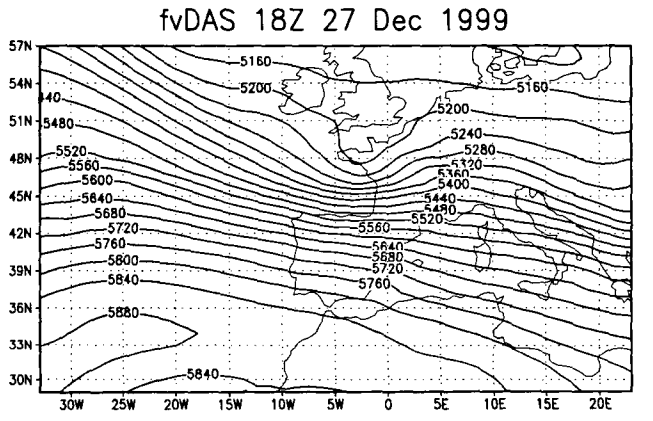

f

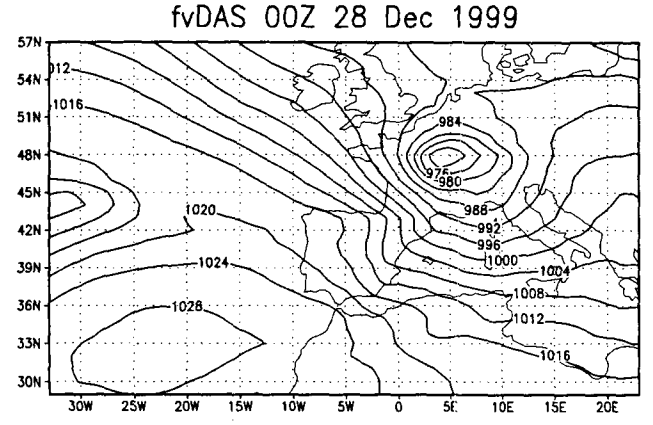

g

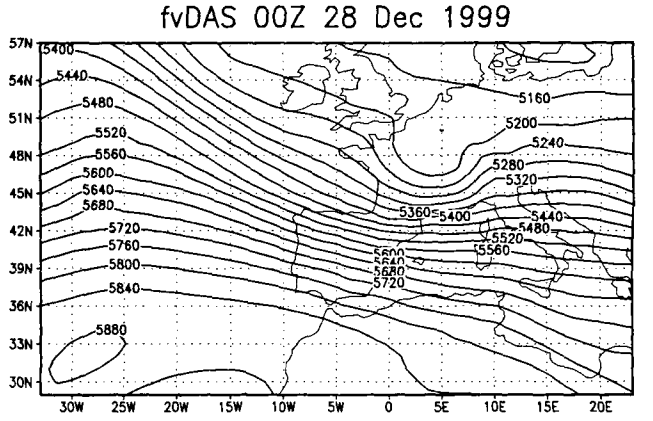

h

Fig 6

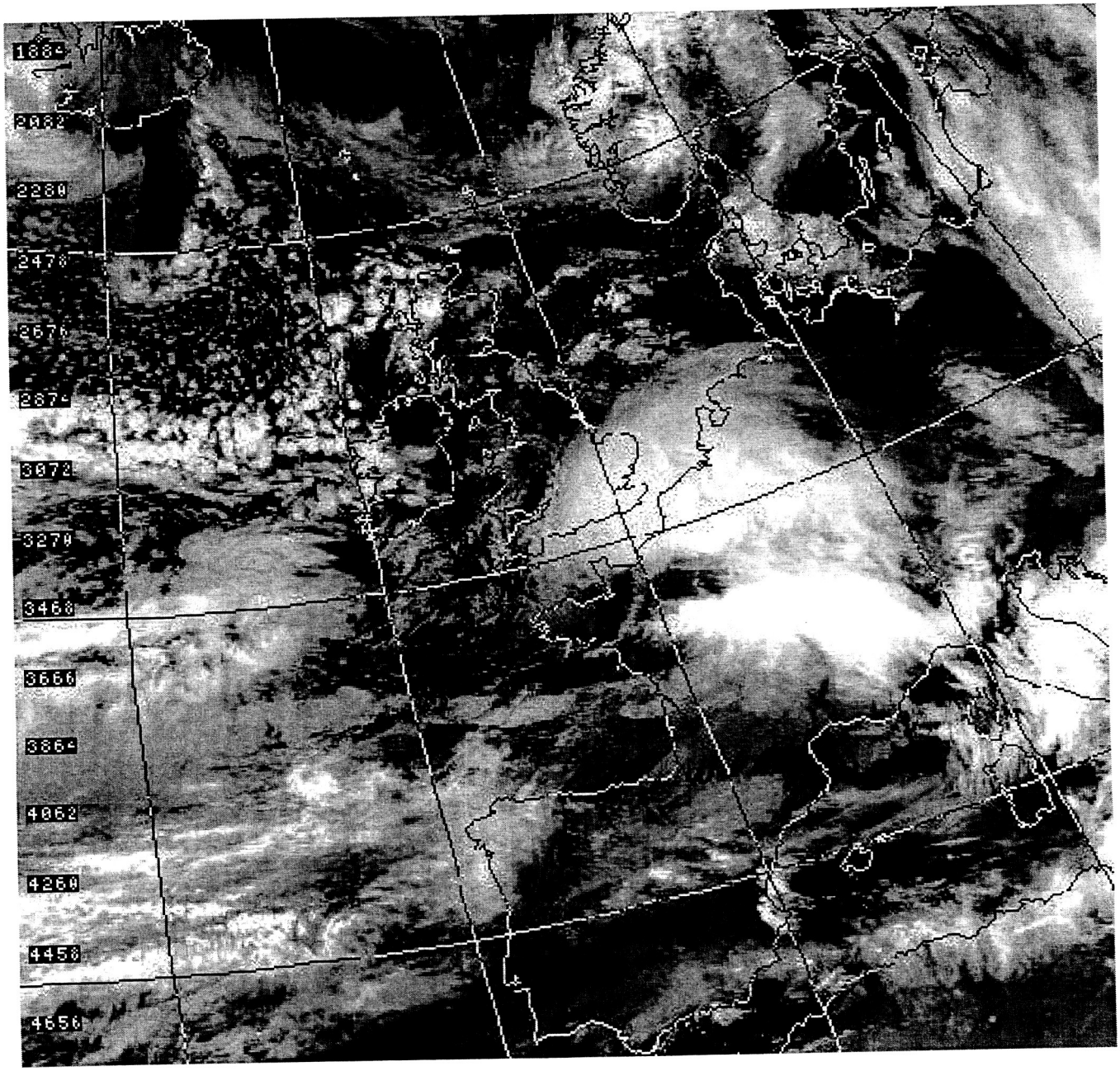
1884
2082
2280
2478
2676
2874
3072
3270
3468
3666
3864
4062
4260
4458
4656

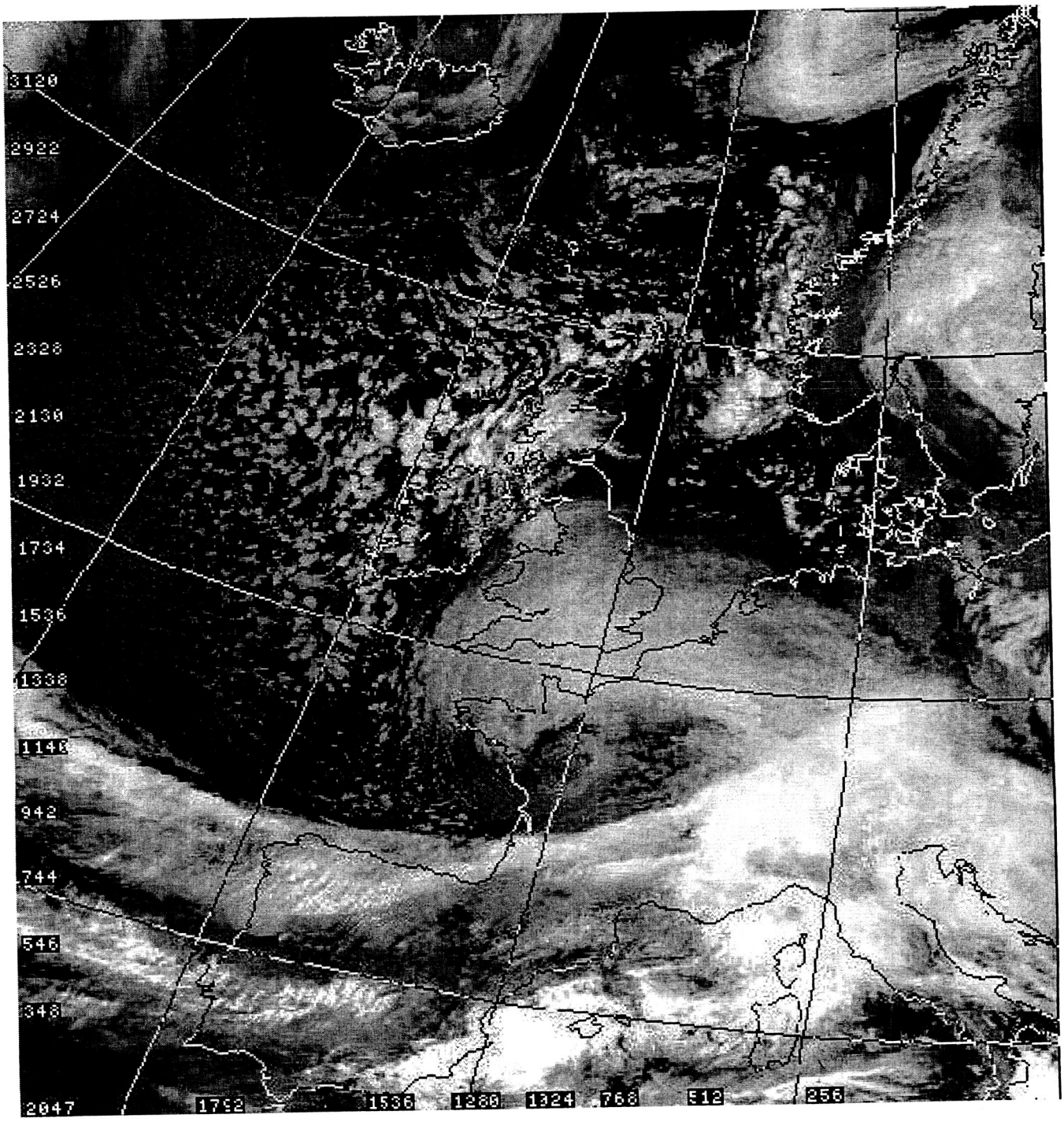
3120
2922
2724
2526
2328
2130
1932
1734
1536
1338
1140
942
744
546
348
2047
1792
1536
1280
1024
768
512
256

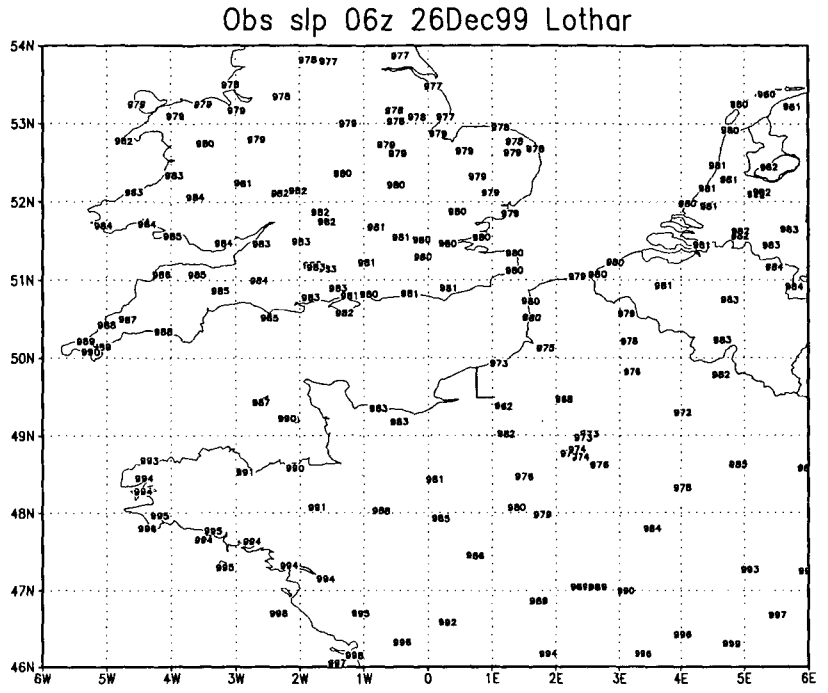
Obs slp 06z 26Dec99 Lothar

a

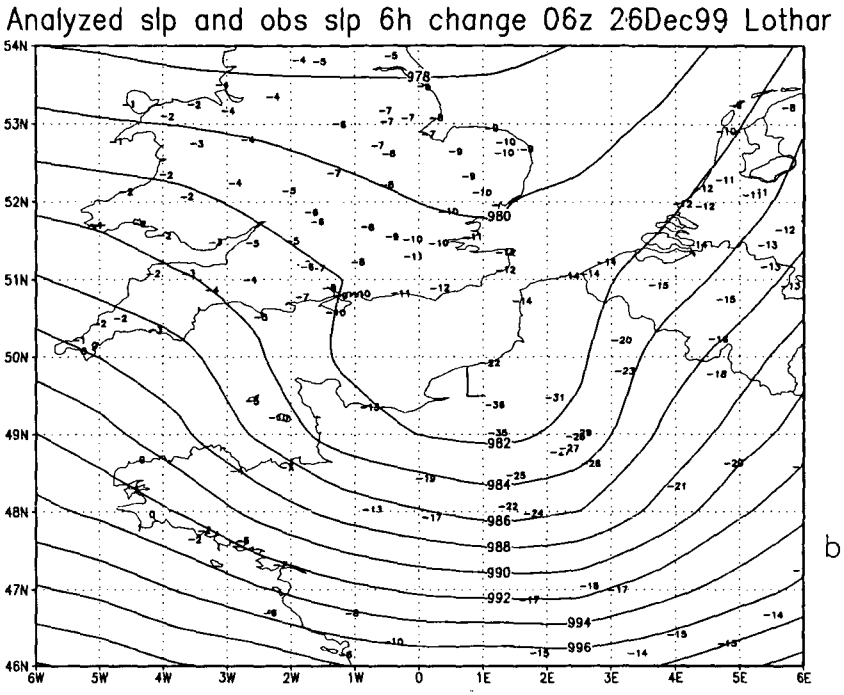
Analyzed slp and obs slp 6h change 06z 26Dec99 Lothar

b

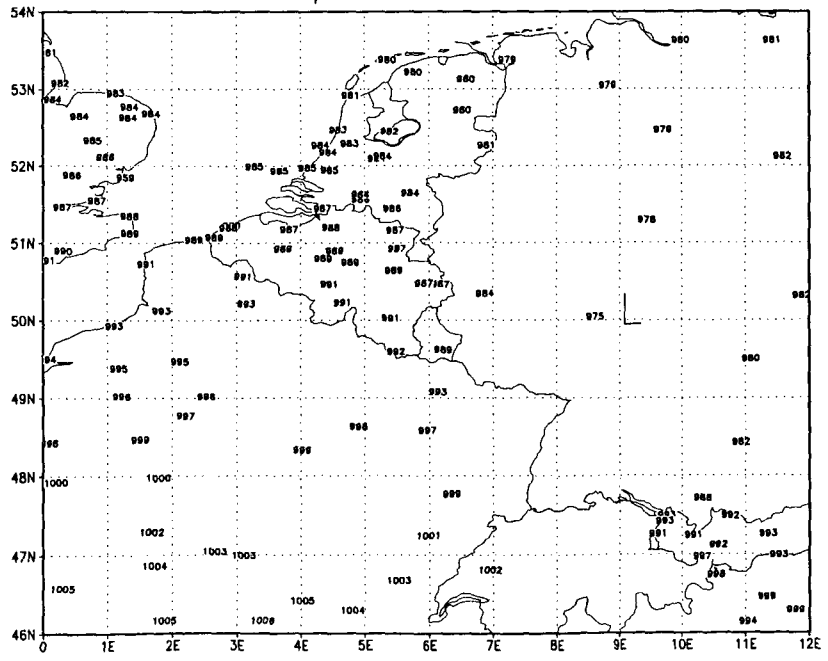
Obs slp 12z 26Dec99 Lothar

c

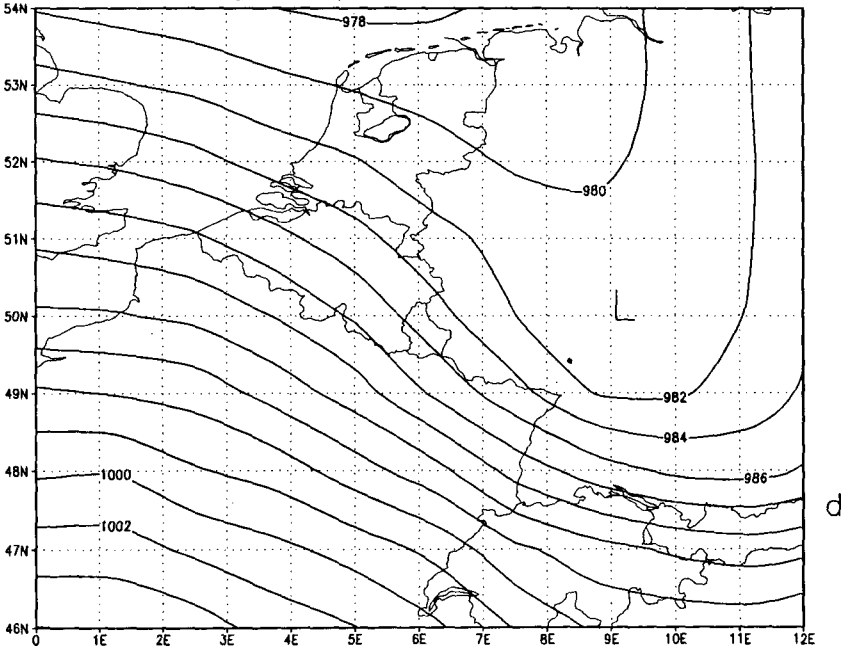
Analyzed slp 12z 26Dec99 Lothar

d

Fig 8

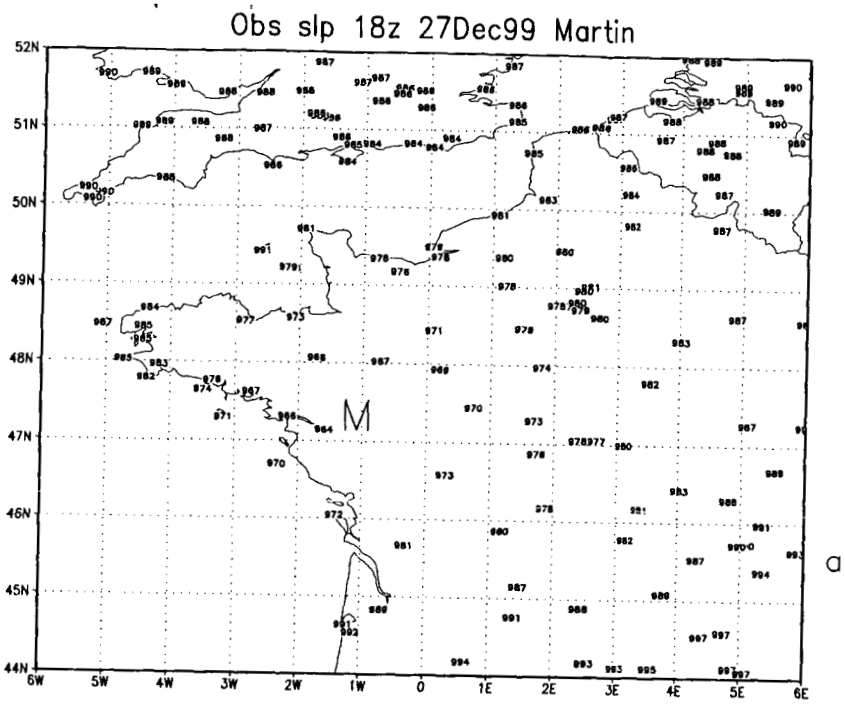
Obs slp 18z 27Dec99 Martin
M

a

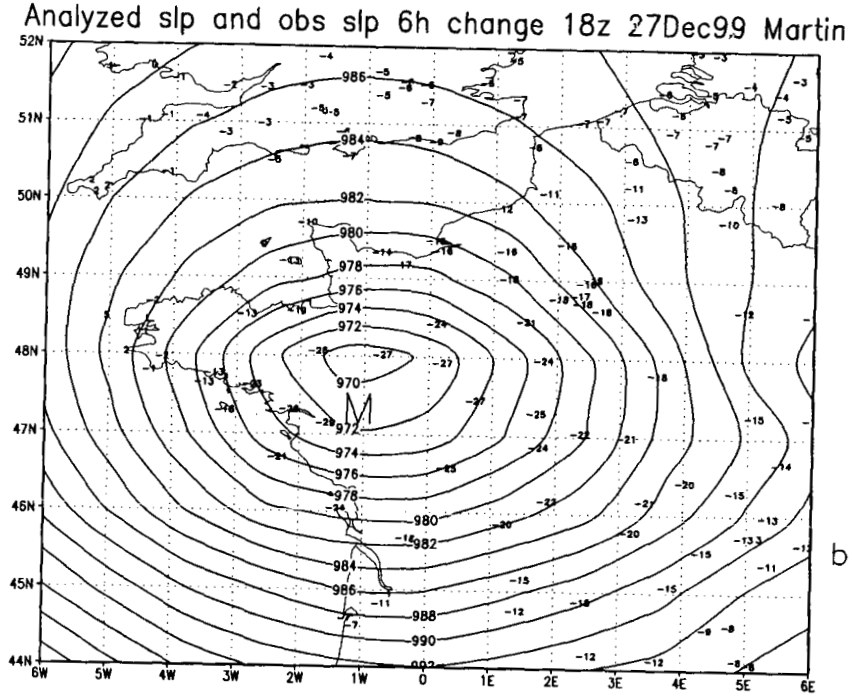
Analyzed slp and obs slp 6h change 18z 27Dec99 Martin
M

b

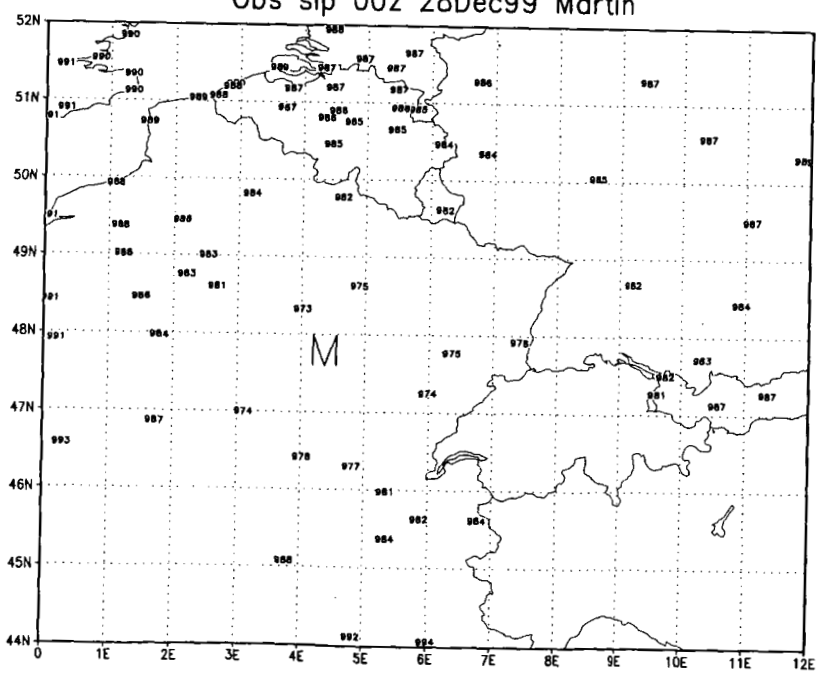
Obs slp 00z 28Dec99 Martin
M

c

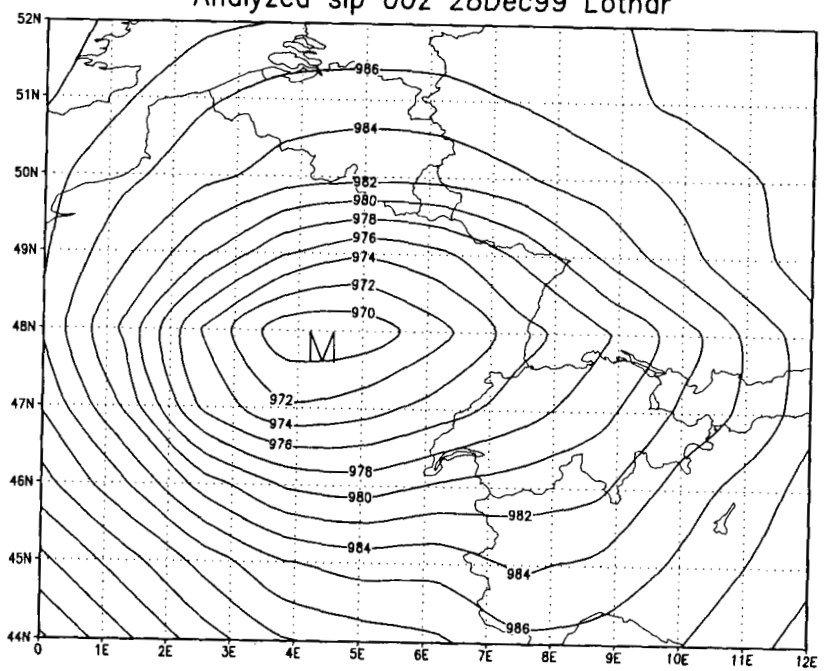
Analyzed slp 00z 28Dec99 Lothar
M

d

Fig 9

06Z 26Dec EXP2 minus EXP1

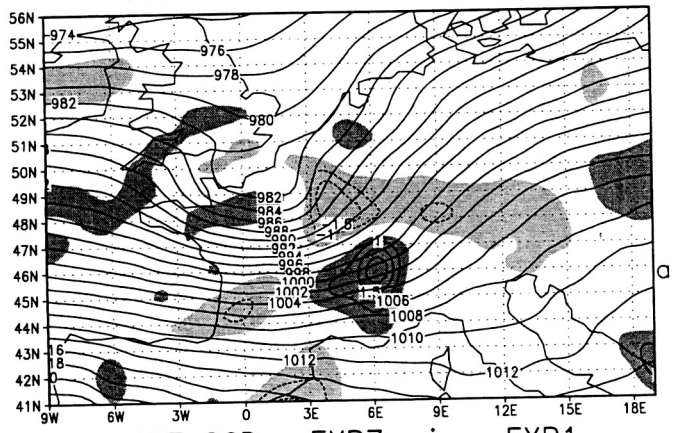

a

06Z 26Dec EXP5 minus EXP1

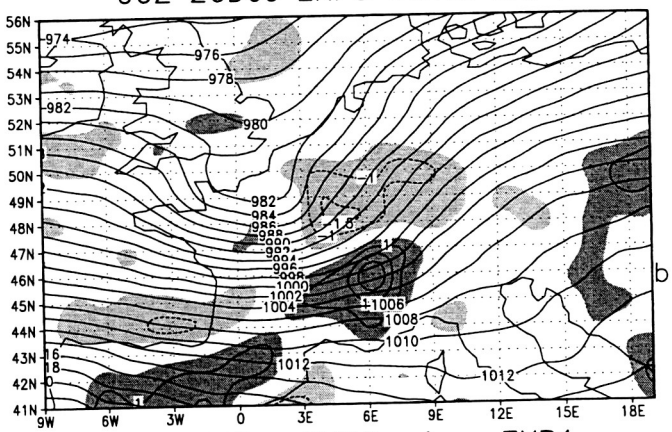

b

06Z 26Dec EXP7 minus EXP1

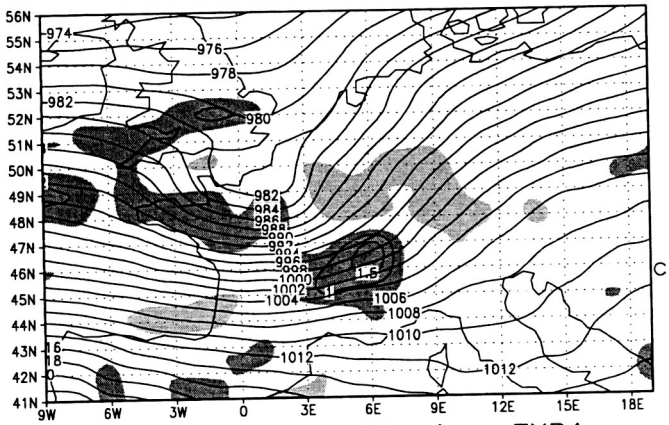

c

06Z 26Dec EXP9 minus EXP1

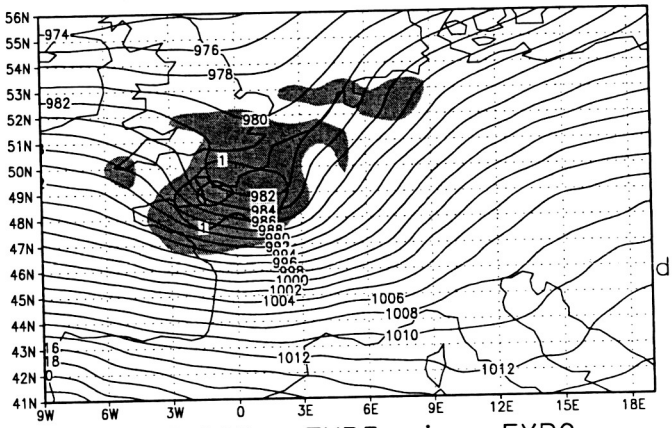

d

06Z 26Dec EXP13 minus EXP1

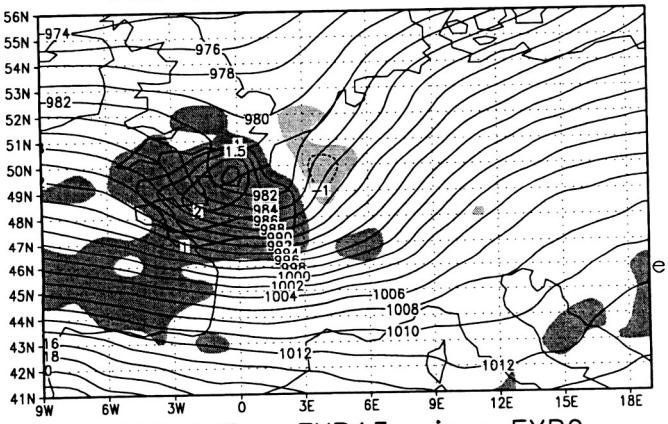

e

06Z 26Dec EXP3 minus EXP9

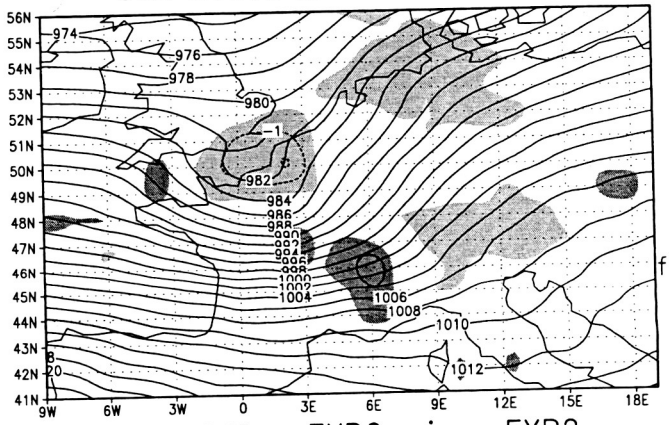

f

06Z 26Dec EXP13 minus EXP9

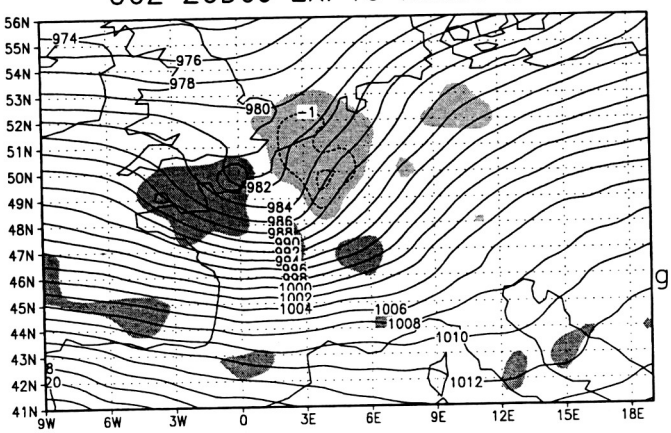

g

06Z 26Dec EXP6 minus EXP2

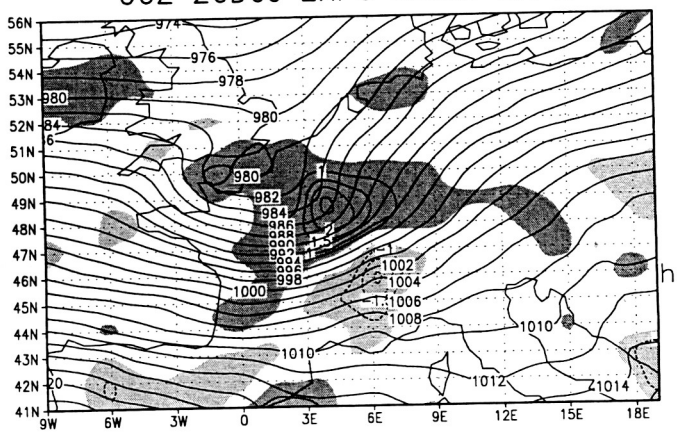

h

Fig 10

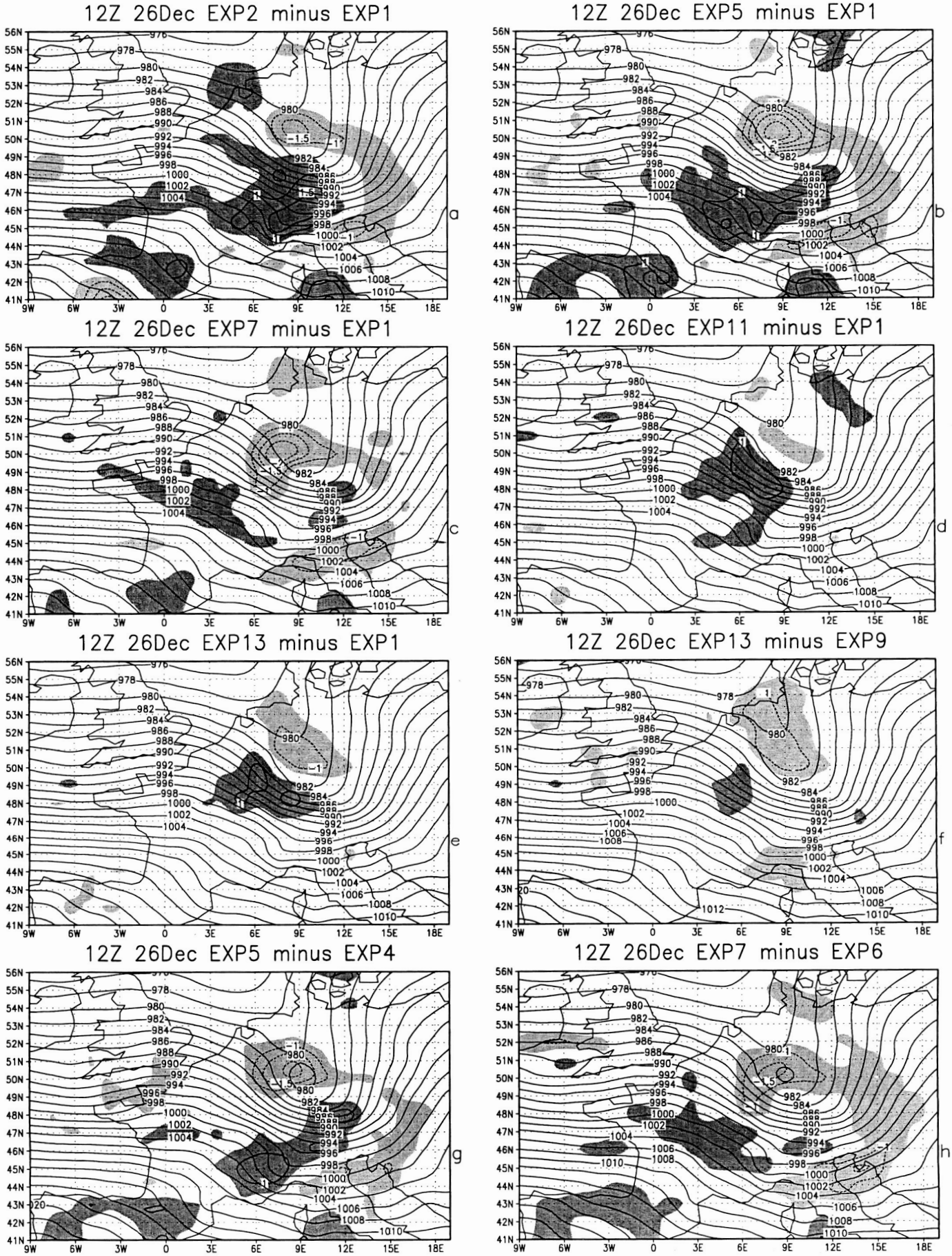
12Z 26Dec EXP2 minus EXP1
12Z 26Dec EXP5 minus EXP1
12Z 26Dec EXP7 minus EXP1
12Z 26Dec EXP11 minus EXP1
12Z 26Dec EXP13 minus EXP1
12Z 26Dec EXP13 minus EXP9
12Z 26Dec EXP5 minus EXP4
12Z 26Dec EXP7 minus EXP6
a
b
c
d
e
f
g
h

Fig 11

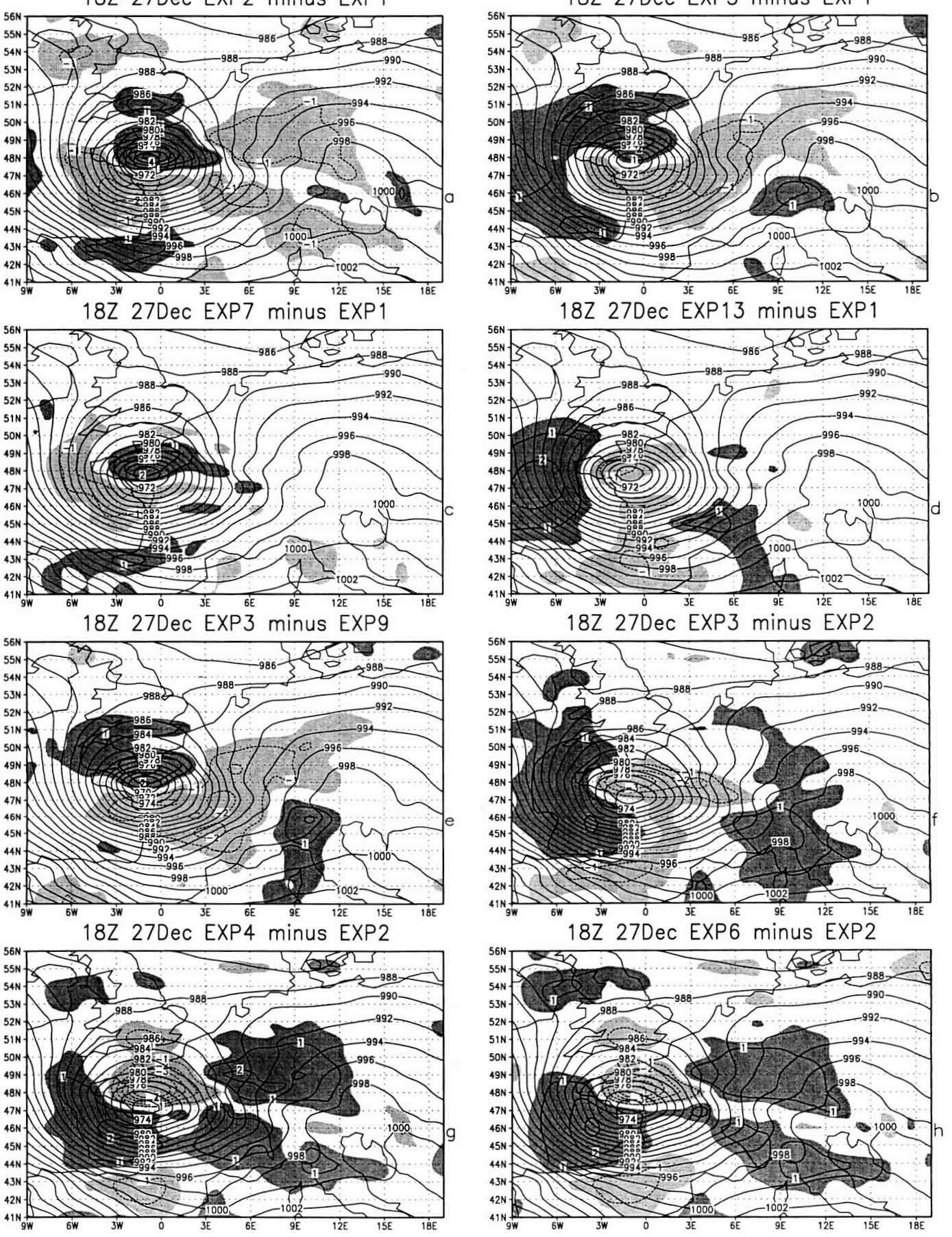
18Z 27Dec EXP2 minus EXP1
a
18Z 27Dec EXP3 minus EXP1
b
18Z 27Dec EXP7 minus EXP1
c
18Z 27Dec EXP13 minus EXP1
d
18Z 27Dec EXP3 minus EXP9
e
18Z 27Dec EXP3 minus EXP2
f
18Z 27Dec EXP4 minus EXP2
g
18Z 27Dec EXP6 minus EXP2
h

Fig 12

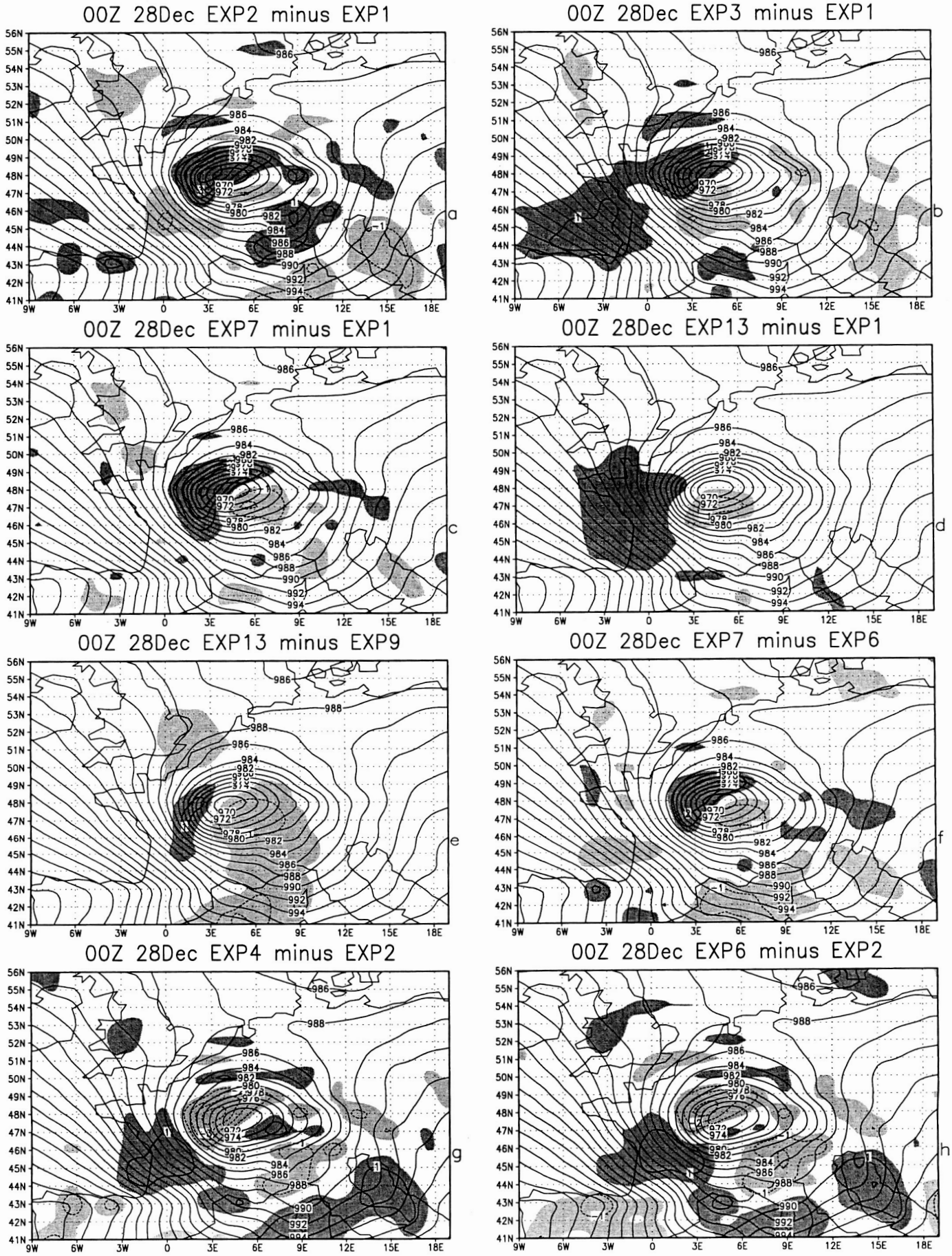
00Z 28Dec EXP2 minus EXP1
a
00Z 28Dec EXP3 minus EXP1
b
00Z 28Dec EXP7 minus EXP1
c
00Z 28Dec EXP13 minus EXP1
d
00Z 28Dec EXP13 minus EXP9
e
00Z 28Dec EXP7 minus EXP6
f
00Z 28Dec EXP4 minus EXP2
g
00Z 28Dec EXP6 minus EXP2
h

Fig 13

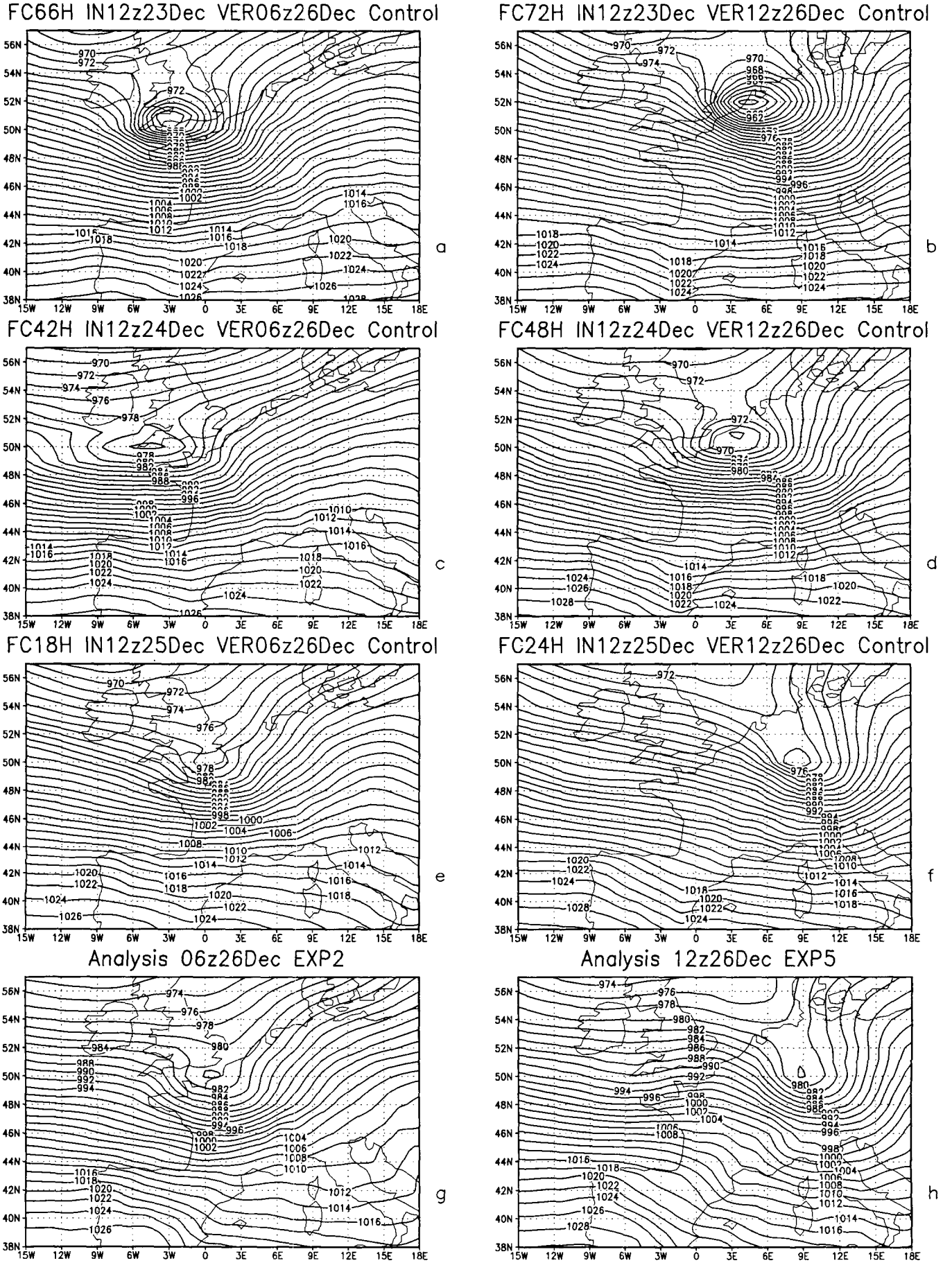
FC66H IN12z23Dec VER06z26Dec Control
a
FC72H IN12z23Dec VER12z26Dec Control
b
FC42H IN12z24Dec VER06z26Dec Control
c
FC48H IN12z24Dec VER12z26Dec Control
d
FC18H IN12z25Dec VER06z26Dec Control
e
FC24H IN12z25Dec VER12z26Dec Control
f
Analysis 06z26Dec EXP2
g
Analysis 12z26Dec EXP5
h

Fig 14

FC72H IN12z23Dec VER12z26Dec EXP13

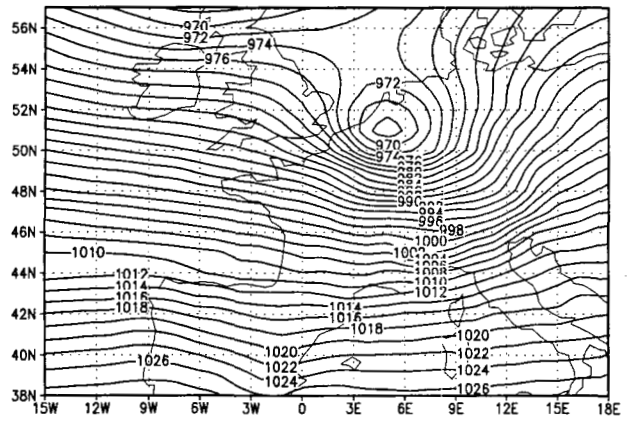

a

FC24H IN12z25Dec VER12z26Dec EXP13

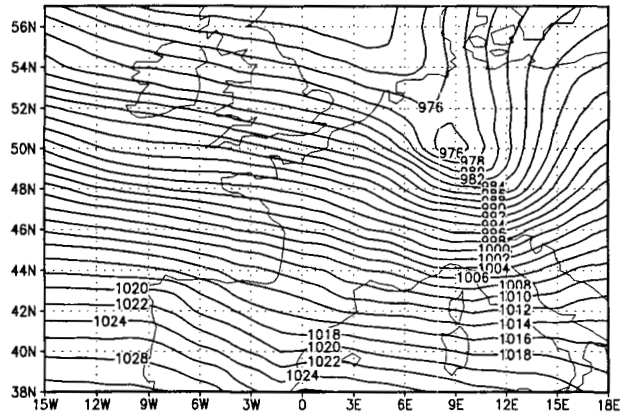

b

FC24H IN12z25Dec VER12z26Dec EXP2

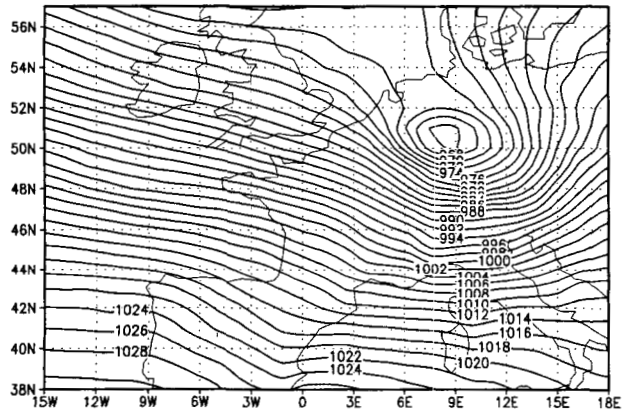

c

Fig 15

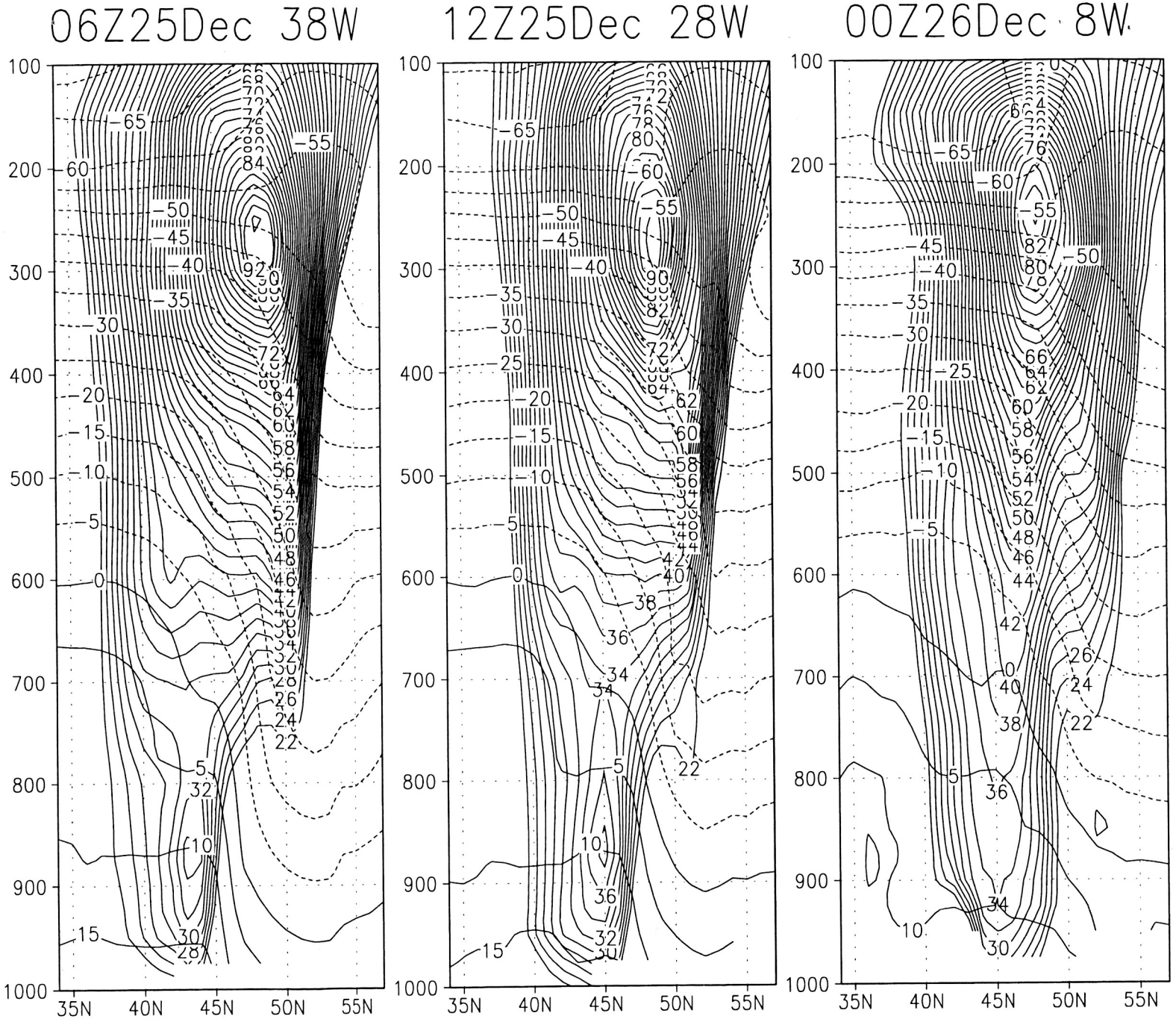
06Z25Dec 38W
12Z25Dec 28W
00Z26Dec 8W
100
200
300
400
500
600
700
800
900
1000
35N
40N
45N
50N
55N

Fig 16

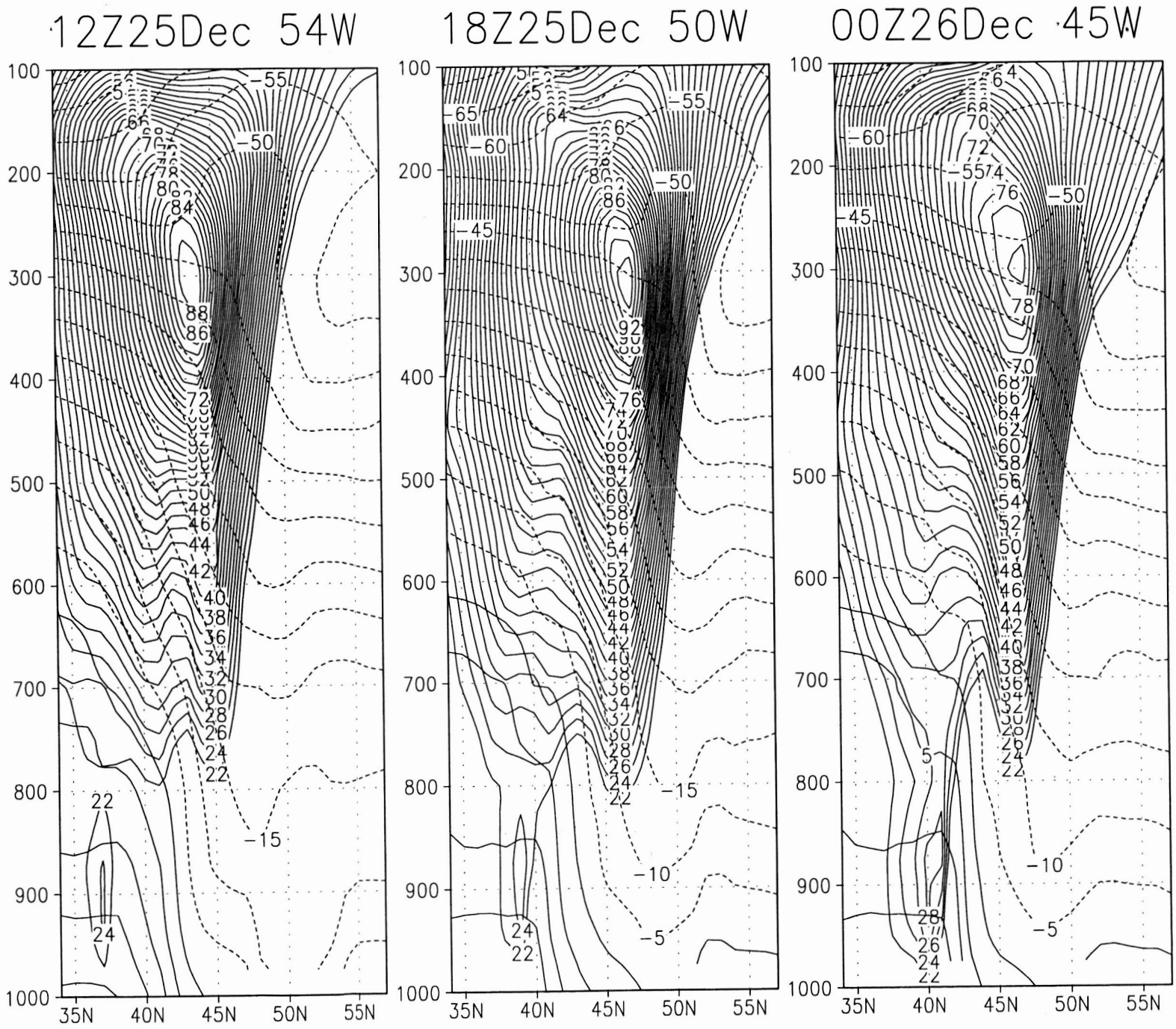
12Z25Dec 54W
18Z25Dec 50W
00Z26Dec 45W
100
200
300
400
500
600
700
800
900
1000
35N
40N
45N
50N
55N

Fig 17

Fig 17

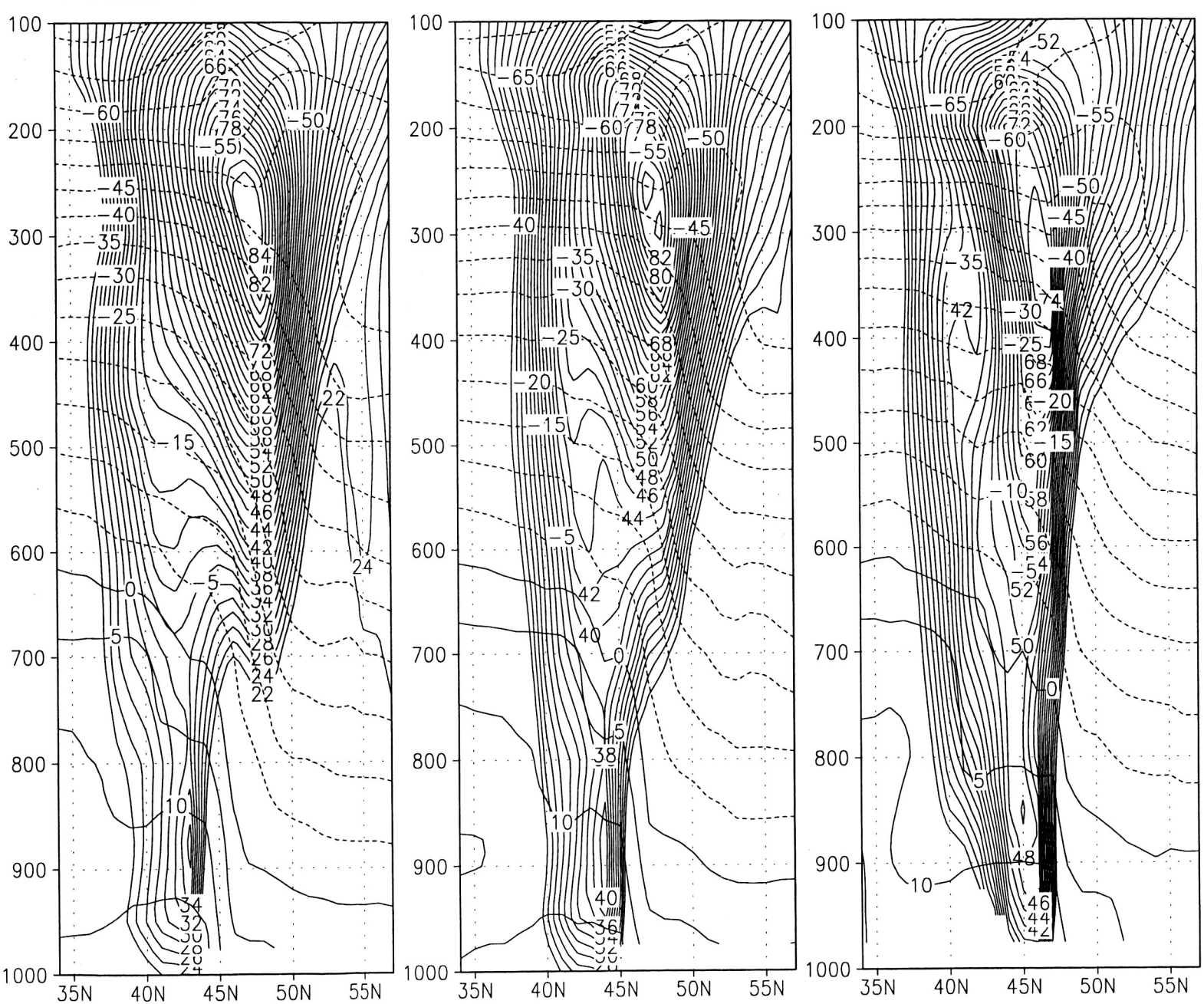
18Z26Dec 35W
00Z27Dec 26W
12Z27Dec 8W
100
200
300
400
500
600
700
800
900
1000
35N
40N
45N
50N
55N

Fig 18

Fig 18

18z25Dec99 300 hPa Eumetsat Winds

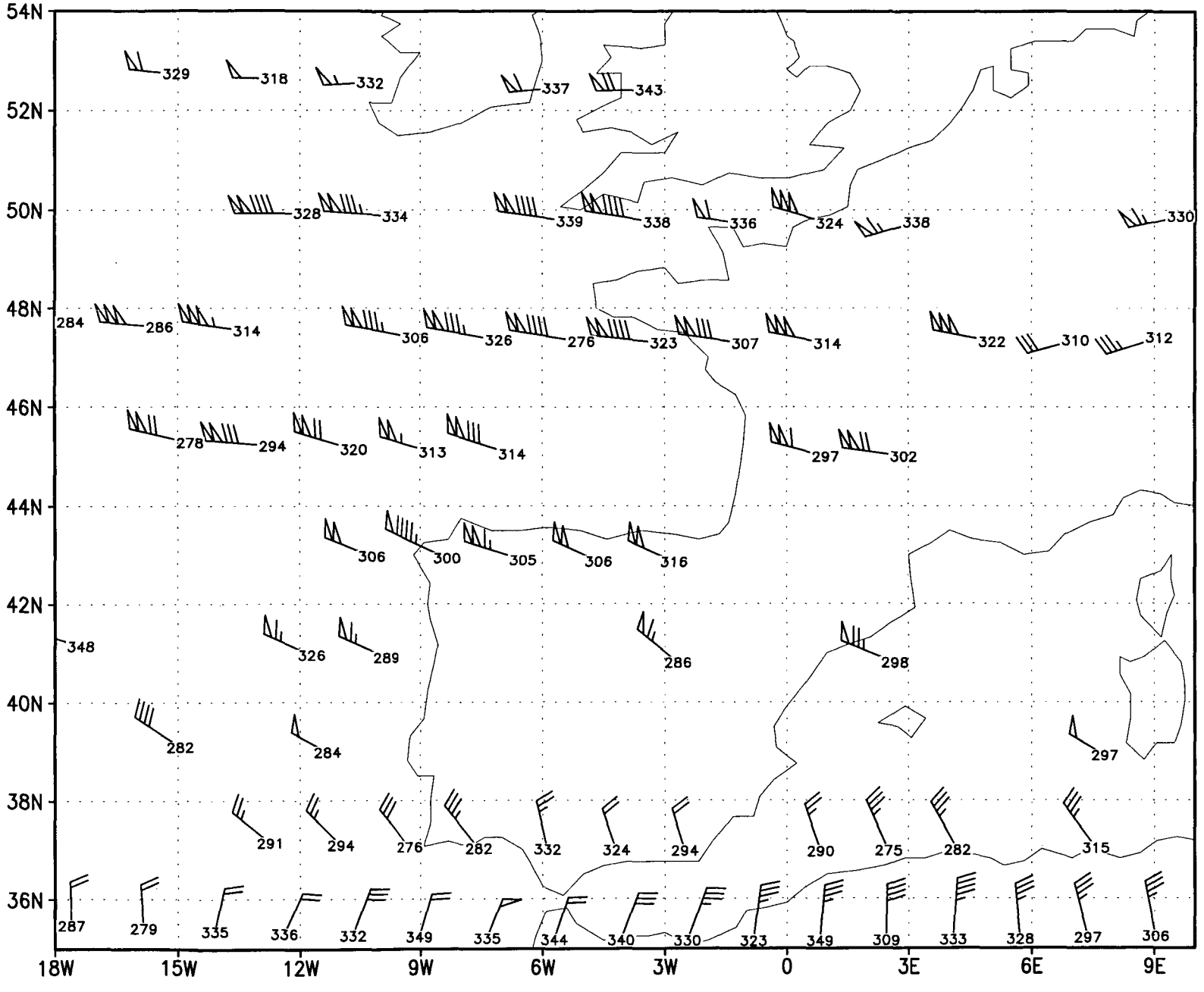

Fig 9

Fig 9